Since January 2020 Elsevier has created a COVID-19 resource centre with free information in English and Mandarin on the novel coronavirus COVID-19. The COVID-19 resource centre is hosted on Elsevier Connect, the company's public news and information website.

Results in Physics 33 (2022) 105177

Contents lists available at ScienceDirect

Results in Physics

journal homepage: www.elsevier.com/locate/rinp

Optimal control and comprehensive cost-effectiveness analysis for COVID-19

Joshua Kiddy K. Asamoah [a,b], Eric Okyere [c], Afeez Abidemi [d], Stephen E. Moore [e], Gui-Quan Sun [a,f,*], Zhen Jin [f], Edward Acheampong [g], Joseph Frank Gordon [h]

[a] Department of Mathematics, North University of China, Taiyuan, Shanxi 030051, China
[b] Department of Mathematics, Kwame Nkrumah University of Science and Technology, Kumasi, Ghana
[c] Department of Mathematics and Statistics, University of Energy and Natural Resources, Sunyani, Ghana
[d] Department of Mathematical Sciences, Federal University of Technology Akure, PMB 704, Ondo State, Nigeria
[e] Department of Mathematics, University of Cape Coast, Cape Coast, Ghana
[f] Complex Systems Research Center, Shanxi University, Shanxi 030006, Taiyuan China
[g] Department of Statistics and Actuarial Science University of Ghana, P.O. Box, LG 115, Legon, Ghana
[h] Department of Mathematics Education, Akenten Appiah Menka University of Skills Training and Entrepreneurial Development, Kumasi, Ghana

ARTICLE INFO

Keywords:
Control strategies
Existence of optimal control
Cost minimizing analysis
Economic health outcomes

ABSTRACT

Cost-effectiveness analysis is a mode of determining both the cost and economic health outcomes of one or more control interventions. In this work, we have formulated a non-autonomous nonlinear deterministic model to study the control of COVID-19 to unravel the cost and economic health outcomes for the autonomous nonlinear model proposed for the Kingdom of Saudi Arabia. We calculated the strength number and noticed the strength number is less than zero, meaning the proposed model does not capture multiple waves, hence to capture multiple wave new compartmental model may require for the Kingdom of Saudi Arabia. We proposed an optimal control problem based on a previously studied model and proved the existence of the proposed optimal control model. The optimality system associated with the non-autonomous epidemic model is derived using Pontryagin's maximum principle. The optimal control model captures four time-dependent control functions, thus, u_1-practising physical or social distancing protocols; u_2-practising personal hygiene by cleaning contaminated surfaces with alcohol-based detergents; u_3-practising proper and safety measures by exposed, asymptomatic and symptomatic infected individuals; u_4-fumigating schools in all levels of education, sports facilities, commercial areas and religious worship centres. We have performed numerical simulations to investigate extensive cost-effectiveness analysis for fourteen optimal control strategies. Comparing the control strategies, we noticed that; Strategy 1 (practising physical or social distancing protocols) is the most cost-saving and most effective control intervention in Saudi Arabia in the absence of vaccination. But, in terms of the infection averted, we saw that strategy 6, strategy 11, strategy 12, and strategy 14 are just as good in controlling COVID-19.

Introduction

The recent worldwide outbreaks of COVID-19 infectious disease has attracted a lot of attention in the mathematical modelling and analysis of the COVID-19. In [1], the basic SEIR epidemic model is used to study and explain some analytical results for the asymptotic and peak values and their characteristic times of the susceptible human populations affected by the highly contagious COVID-19 disease. A SLIAR-type epidemic model is used to study COVID-19 infections in China [2]. Estimated basic reproduction numbers for the COVID-19 infectious disease transmission dynamics in Italy and China have been carried out in [3], using a modified classical SIR mathematical model characterized by time-dependent transmission rates. A prediction and data-driven based SEIRQ COVID-19 nonlinear infection model is formulated and studied in [4]. The authors in [5] have developed and analysed a non-linear epidemic model to explain the spreading dynamics of the 2019 coronavirus among the susceptible human population, the environment as well as wild animals. Two novel data-driven compartmental models are proposed in [6,7] to investigate the COVID-19 pandemic in South Africa.

* Corresponding author.
E-mail addresses: topeljoshua@gmail.com (J.K.K. Asamoah), eric.okyere@uenr.edu.gh (E. Okyere), aabidemi@futa.edu.ng (A. Abidemi), stephen.moore@ucc.edu.gh (S.E. Moore), sunguiquan@sxu.edu.cn (G.-Q. Sun), jinzhn@263.net (Z. Jin), eoacheampong@ug.edu.gh (E. Acheampong), jfgordon@aamusted.edu.gh (J.F. Gordon).

https://doi.org/10.1016/j.rinp.2022.105177
Received 18 February 2021; Received in revised form 23 December 2021; Accepted 3 January 2022
Available online 15 January 2022

Mathematical modelling tools are essential in studying infectious diseases epidemiology because they can at least give some insight into the spreading dynamics of disease outbreaks and help in suggesting possible control strategies. Atangana, proposed a mathematical model that demonstrates fractional calculus's survival. Six classes were taken into account, and all basic analyses were presented. In addition, a novel analysis was proposed that includes a strength number that accounts for the accelerative information of nonlinear and linear parts of a specific epidemiological model [8]. The authors in [9] have constructed and analysed a non-autonomous differential equation model by introducing medical mask, isolation, treatment, and detergent spray as time-dependent controls. Global parameter sensitivity analysis for a new COVID-19 differential equation model is carried out in the work of Ali and co-authors [10]. They also proposed and analysed a non-autonomous epidemic model for the COVID-19 disease in the same work using quarantine and isolation as time-dependent control functions. Atangana and Araz [11] presented a mathematical studies on forecasting the spread of COVID-19 in Africa and Europe using stochastic and deterministic approaches. They asserted that their model can forecast two to three waves of the spread in the near future. The work in [12] studied mathematical analysis of the effects of controls on transmission dynamics of SARS-CoV-2. The spread of COVID-19 with new fractal–fractional operators with the impose of lockdown saving mankind before vaccination is presented in [13]. Furthermore, a COVID-19 mathematical is studied in recent work by the authors in [14], where they considered three time-dependent control functions consisting of preventive control measures (quarantine, isolation, social distancing), disinfection of contaminated surfaces to reduce intensive medical care and infected individuals in the population. A non-optimal and optimal control deterministic COVID-19 models are studied in [15]. The authors explored control and preventive interventions such as rapid testing, medical masks, improvement of medical treatment in hospitals, and community awareness. An optimal control nonlinear epidemic model for COVID-19 infection that captures optimal preventive and control strategies such as personal protection measures, treatment of hospitalized individuals, and public health education is formulated and analysed to study the dynamics of the epidemic in Ethiopia [16]. Optimal Control analysis for the 2019 coronavirus epidemic has been studied using non-pharmaceutical control and preventive interventions to examine the dynamics of the disease in the USA [17]. The work in [18] studied a fractional-order mathematical model for COVID-19 dynamics with quarantine, isolation, and environmental viral load. Asamoah et al. [19] presented a COVID-19 model to study the impact of the environment on the spread of the disease in Ghana. They further investigated the economic outcomes using cost-effectiveness analysis. Alqarni [20] formulated and analysed a novel deterministic COVID-19 epidemic model characterized by nonlinear differential equations with six state variables to describe the COVID-19 dynamics in the Kingdom of Saudi Arabia. They gave a detailed qualitative stability analysis and also determined the influential model parameters on the basic reproduction number, $\mathcal{R}_0$, using global sensitivity analysis. They further performed numerical simulations to support their theoretical results, following their novel mathematical modelling formulation, analysis, and the generated global sensitivity analysis results. In recent times, cost-effectiveness analysis of epidemic optimal control models has become very important in suggesting realistic optimal control strategies to help reduce the spread of infectious diseases in limited-resource settings. Also, assessing the amount it cost to acquire a unit of a health outcome like infection averted, susceptibility prevented, life-year gained, or death prevented, and the expenses and well-being results of at least one or more interventions. In the work [21] it has been shown that border closure (or, at the very least, screening) is critical in the battle against the spread of SARS-CoV-2. The model's optimal control simulation reveals that the best cost-effective technique for combating SARS-CoV-2 is to restrict contact via the use of nasal masks and physical separation. Asamoah and colleagues [22] investigated optimal control and cost-effectiveness analysis. Their key result is that having two controls (transmission reduction and case isolation) is better than having one, although it is more costly. Transmission reduction is preferable to case isolation when just one control is available. Omame et al. [23] developed and analysed a mathematical model for the dynamics of COVID-19 with re-infection in order to evaluate the influence of past comorbidity (particularly, diabetes mellitus) on COVID-19 complications. Furthermore, the model's optimal control and cost-effectiveness analyses show that the approach that avoids COVID-19 infection by comorbid susceptibles is the most cost-effective of all COVID-19 control options considered by the authors. Therefore, motivated by the above researches, this work presents a cost-effectiveness analysis for the study in [20]. The rest of the paper is organized as follows: "The autonomous model" presents the general description of the model states, and transition terms from Alqarni [20], "Optimal control problem formulation and analysis of COVID-19 model" gives the bases for the formulation of the optimal control model, the proof of existence and the characterization of the optimal control problem. "Numerical simulation and cost-effectiveness analysis" contains the numerical simulations for the various control strategies and cost-effectiveness analysis. "Concluding remarks" contain the concluding remarks.

The autonomous model

The formulated model is divided into five distinct human compartments, identified as, the susceptible, $S(t)$, exposed, $E(t)$, asymptomatic infected (not showing symptoms but can infect other healthy people) $A(t)$, symptomatic infected (that have symptoms of disease and can infect other people) $I(t)$, and the recovered individuals, $R(t)$, where the total population is given as $N(t) = S(t) + E(t) + A(t) + I(t) + R(t)$. The assumed concentration of the SARS-CoV-2 in the environment is denoted by $B(t)$. Individuals in the infected classes $E(t), A(t), I(t)$ are assumed of transmitting the disease to the susceptible individuals at the rate $\beta_1, \beta_2, \beta_3$, respectively, and β_4 is the propensity rate of susceptible individuals getting the virus through the environment. The set of differential equations for the autonomous system is given as

$$\begin{aligned}
\frac{dS}{dt} &= \Lambda - \left(\beta_1 E + \beta_2 I + \beta_3 A\right)\frac{S}{N} - \beta_4 B\frac{S}{N} - dS,\\
\frac{dE}{dt} &= \left(\beta_1 E + \beta_2 I + \beta_3 A\right)\frac{S}{N} + \beta_4 B\frac{S}{N} - (\delta + d)E,\\
\frac{dI}{dt} &= (1-\tau)\delta E - (d + d_1 + \gamma_1)I,\\
\frac{dA}{dt} &= \tau\delta E - (d + \gamma_2)A,\\
\frac{dR}{dt} &= \gamma_1 I + \gamma_2 A - dR,\\
\frac{dB}{dt} &= \psi_1 E + \psi_2 I + \psi_3 A - \phi B,
\end{aligned} \tag{1}$$

with the initial conditions

$$\begin{aligned}
&S(0) = S_0 > 0, E(0) = E_0 \geq 0, I(0) = I_0 \geq 0,\\
&A(0) = A_0 \geq 0, R(0) = R_0 \geq 0, B(0) = B_0 \geq 0.
\end{aligned}$$

The model's recruitment rate is given as Λ with d representing the natural death rate. The Greek symbols $\beta_1, \beta_2, \beta_3$, are the respective direct transmission rates among exposed and susceptible individuals, infected (showing symptoms) and susceptible individuals, symptomatically infected (not showing symptoms) and susceptible individuals, and β_4 is the indirect transmission of the virus to the susceptible individuals. The rate at which the exposed individuals develops symptoms become infected is denoted as $(1-\tau)\delta$, where the rate of new asymptomatic infection is represented as $\tau\delta$. The disease-induced death rate is denoted as d_1. Here, the symptomatic, asymptomatic recovery rate is epidemiological assumed as γ_1 and γ_2, respectively. Furthermore, the epidemiological rates for shedding the virus into the environment by the exposed, infected and asymptomatically infected people is denoted

as ψ_1, ψ_2 and ψ_3 respectively. The rate of natural removal of the virus from the environment is denoted as ϕ. Alqarni et al. [20] gave the basic reproduction expression, detailed qualitative stability analysis and also determined the influential model parameters on the basic reproduction number, $\mathcal{R}_0$, using global sensitivity analysis. They further performed numerical simulations to support their theoretical results. The basic reproduction number from Alqarni et al. [20] is given as

$$\mathcal{R}_0 = \frac{k_2(\delta\tau(\beta_4\psi_3 + \beta_3\phi) + k_3(\beta_4\psi_1 + \beta_1\phi)) + \delta k_3(1-\tau)(\beta_4\psi_2 + \beta_2\phi)}{k_1 k_2 k_3 \phi}, \quad (2)$$

where $k_1 = d+\delta, k_2 = \gamma_1 + d + d_1$ and $k_3 = \gamma_2 + d$. Following their global sensitivity result of the basic reproduction number, "Optimal control problem formulation and analysis of COVID-19 model" is conceived. Before then, one can calculate the strength number of the above autonomous model (1). From [8] the strength number may accounts for the accelerative information of a specific epidemiological model's nonlinear and linear elements.

Strength number

In recent decades, the idea of reproduction number has been extensively used in epidemiological modelling since it has been recognized as a helpful mathematical formula for evaluating new infections. According to the theory, one will identify two components from the proposed model's infectious compartments, where $\mathcal{F}$ is the matrix that contain the new infections and $\mathcal{V}$ is the matrix that contain the transition elements. Then,

$$\left(\mathcal{F}\mathcal{V}^{-1} - \lambda^* I\right) = 0 \quad (3)$$

gives the reproduction number [24], here λ^* is the eigenvalue and I is an identity matrix. Now following directly from [8], the component $\mathcal{F}$ is derived from the nonlinear component of the infected compartments:

$$\frac{\partial}{\partial E}\left(\frac{E}{N}\right) = \frac{N-E}{N^2}, \quad \frac{\partial}{\partial I}\left(\frac{I}{N}\right) = \frac{N-I}{N^2},$$
$$\frac{\partial}{\partial A}\left(\frac{A}{N}\right) = \frac{N-A}{N^2}, \quad \frac{\partial}{\partial B}\left(\frac{B}{N}\right) = \frac{1}{N}.$$

As defined before, S is the susceptible individuals, E is exposed individuals assumed infectious, A is asymptomatic infected individuals (not showing symptoms but can infect other healthy people), while I is the symptomatic infected individuals (that have symptoms of disease and can infect other people). The assumed concentration of the SARS-CoV-2 in the environment is denoted by B. Furthermore, we have

$$\frac{\partial^2}{\partial E^2}\left(\frac{N-E}{N^2}\right) = \frac{-2(N-E)}{N^3}, = \frac{-2(S+I+A+R)}{(S+E+I+A+R)^3},$$
$$\frac{\partial^2}{\partial I^2}\left(\frac{N-I}{N^2}\right) = \frac{-2(N-I)}{N^3}, = \frac{-2(S+E+A+R)}{(S+E+I+A+R)^3},$$
$$\frac{\partial^2}{\partial A^2}\left(\frac{N-A}{N^2}\right) = \frac{-2(N-A)}{N^3}, = \frac{-2(S+E+I+R)}{(S+E+I+A+R)^3},$$
$$\frac{\partial^2}{\partial B^2}\left(\frac{1}{N}\right) = 0.$$

From [20] the model has a unique disease free equilibrium, given by

$$\left(S_0, E_0, I_0, A_0, R_0, B_0\right) = \left(\frac{\Lambda}{d}, 0, 0, 0, 0, 0\right).$$

Hence, at the disease-free equilibrium, we have

$$\frac{-2(S_0+I_0+A_0+R_0)}{(S_0+E_0+I_0+A_0+R_0)^3} = -\frac{2}{{S_0}^2},$$
$$\frac{-2(S_0+E_0+A_0+R_0)}{(S_0+E_0+I_0+A_0+R_0)^3} = -\frac{2}{{S_0}^2},$$
$$\frac{-2(S_0+E_0+I_0+R_0)}{(S_0+E_0+I_0+A_0+R_0)^3} = -\frac{2}{{S_0}^2}.$$

In this scenario, we have the following for $\mathcal{F}$ and $\mathcal{V}$:

$$\mathcal{F}_{\mathcal{A}} = \begin{pmatrix} -\frac{2\beta_1 d}{\Lambda} & -\frac{2\beta_2 d}{\Lambda} & -\frac{2\beta_3 d}{\Lambda} & 0 \\ 0 & 0 & 0 & 0 \\ 0 & 0 & 0 & 0 \\ 0 & 0 & 0 & 0 \end{pmatrix},$$
$$\mathcal{V} = \begin{pmatrix} (\delta+d) & 0 & 0 & 0 \\ -(1-\tau)\delta & (d+d_1+\gamma_1) & 0 & 0 \\ -\tau\delta & 0 & (d+\gamma_2) & 0 \\ -\psi_1 & -\psi_2 & -\psi_3 & \phi \end{pmatrix}. \quad (4)$$

Then from (3), we get

$$\left(\mathcal{F}_A \mathcal{V}^{-1} - \lambda^* I\right) = 0, \quad (5)$$

which leads to

$$A_0 = -\frac{2\beta_1 d}{\Lambda(d+\delta)} - \frac{2\beta_2 d(\delta - \delta\tau)}{\Lambda(d+\delta)(d+d_1+\gamma_1)} - \frac{2\beta_3 d^2 \tau}{\Lambda(d+\delta)(d+\gamma_2)} < 0.$$

From the parameters values in Table 1 we have $A_0 = -3.8670 \times 10^{-8}$. $A_0 = 0$ indicates that the spread will not have a renewal process and will consequently have a single magnitude and die out. $A_0 > 0$ indicates that there is sufficient strength to initiate the renewal phase, implying that the spread will have more than one wave. Therefore, we noticed that the model proposed in [20] does not capture the multiple waves of COVID-19.

Optimal control problem formulation and analysis of COVID-19 model

In section 4.1 of the work in Alqarni et al. [20]. They found out that the most sensitive parameters in their basic reproduction number are: Contact rate among exposed and susceptible, β_1, contact rate among environment and susceptible, β_4, virus contribution due to state E to compartment B, ψ_1, and virus removal from the environment, θ. Therefore, to contribute the research knowledge on COVID-19 in Saudi Arabia, we incorporated the following control terms to study the most effective economic and health outcomes in combating this disease which has caused economic hardship in many countries.

Formulation of the non-autonomous COVID-19 model

- u_1: practising physical or social distancing protocols.
- u_2: practising personal hygiene by cleaning contaminated surfaces with alcohol based detergents.
- u_3: practising proper and safety measures by exposed, asymptomatic infected and symptomatic infected individuals.
- u_4: fumigating schools in all levels of education, sports facilities, commercial areas and religious worship centres.

Hence, based on [20], our optimal control model of is given as

$$\frac{dS}{dt} = \Lambda - (1-u_1(t))\left(\beta_1 E + \beta_2 I + \beta_3 A\right)\frac{S}{N} - (1-u_1(t)-u_2(t))\beta_4 B\frac{S}{N} - dS,$$
$$\frac{dE}{dt} = (1-u_1(t))\left(\beta_1 E + \beta_2 I + \beta_3 A\right)\frac{S}{N} + (1-u_1(t) - u_2(t))\beta_4 B\frac{S}{N} - (\delta+d)E,$$
$$\frac{dI}{dt} = (1-\tau)\delta E - (d+d_1+\gamma_1)I, \quad (6)$$

$$\frac{dA}{dt} = \tau\delta E - (d+\gamma_2)A,$$
$$\frac{dR}{dt} = \gamma_1 I + \gamma_2 A - dR,$$
$$\frac{dB}{dt} = (1-u_3(t))\psi_1 E + (1-u_3(t))\psi_2 I + (1-u_3(t))\psi_3 A - (u_4(t)+\phi)B,$$

Formulation of the objective functional

In line with the standard in literature [25–34], the control cost is measures by implementing a quadratic performance index or objective functional in this work. Thus, our goal is to minimize the objective functional, $\mathcal{J}$, given as

$$\mathcal{J}(u_1,u_2,u_3,u_4) := \min \int_0^T \left[A_1E + A_2I + A_3A + A_4B + \frac{1}{2}\sum_{i=1}^{4} D_i u_i^2(t)\right]dt \quad (7)$$

subject to the non-autonomous system (6), where $A_i > 0$ $(i = 1,2,3,4)$ are the balancing weight constants on the exposed, asymptomatic and symptomatic infected individuals, and the concentration of corona virus in the environment respectively, whereas $D_i > 0$ are the balancing cost factors on the respective controls u_i (for $i = 1,\dots,4$), T is the final time for controls implementation.

Suppose $\mathcal{U}$ is a non-empty control set defined by

$$\mathcal{U} = \left\{(u_1,u_2,u_3,u_4) : u_i \text{ Lebesgue measurable},\ 0 \le u_i \le 1,\right.$$
$$\left.\text{for } i = 1,\dots,4,\ t \in [0,T]\right\}. \quad (8)$$

Then, it is of particular interest to seek an optimal control quadruple $u^* = (u_1^*, u_2^*, u_3^*, u_4^*)$ such that

$$\mathcal{J}(u^*) = \min\left\{\mathcal{J}(u_1,u_2,u_3,u_4) : u_1,u_2,u_3,u_4 \in \mathcal{U}\right\}. \quad (9)$$

Existence of an optimal control

Theorem 1. *Given the objective functional $\mathcal{J}$ defined on the control set $\mathcal{U}$ in (8), then there exists an optimal control quadruple $u^* = (u_1^*, u_2^*, u_3^*, u_4^*)$ such that (9) holds when the following conditions are satisfied [35–37]:*

(i) The admissible control set $\mathcal{U}$ is convex and closed.
(ii) The state system is bounded by a linear function in the state and control variables.
(iii) The integrand of the objective functional $\mathcal{J}$ in (7) is convex in respect of the controls.
(iv) The Lagrangian is bounded below by

$$a_0\left(\sum_{i=1}^{4}|u_i|^2\right)^{\frac{a_2}{2}} - a_1,$$

where $a_0, a_1 > 0$ and $a_2 > 1$.

Proof. Let the control set $\mathcal{U} = [0,u_{\max}]^4, u_{\max} \le 1$, $u = (u_1,u_2,u_3,u_4) \in \mathcal{U}$, $x = (S,E,I,A,R,B)$ and $f_0(t,x,u)$ be the right-hand side of the non-autonomous system (6) given by

$$f_0(t,x,u) = \begin{pmatrix} \Lambda - (1-u_1)\frac{(\beta_1E+\beta_2I+\beta_3A)S}{N} - (1-u_1-u_2)\frac{\beta_4BS}{N} - dS \\ (1-u_1)\frac{(\beta_1E+\beta_2I+\beta_3A)S}{N} + (1-u_1-u_2)\frac{\beta_4BS}{N} - (\delta+d)E \\ (1-\tau)\delta E - (d+d_1+\gamma_1)I \\ \tau\delta E - (d+\gamma_2)A \\ \gamma_1 I + \gamma_2 A - dR \\ (1-u_3)\psi_1 E + (1-u_3)\psi_2 I + (1-u_3)\psi_3 A - (u_4+\phi)B \end{pmatrix}. \quad (10)$$

Then, we proceed by verifying the four properties presented by Theorem 1.

(i) Given the control set $\mathcal{U} = [0,u_{max}]^4$. Then, by definition, $\mathcal{U}$ is closed. Further, let $v,w \in \mathcal{U}$, where $v = (v_1,v_2,v_3,v_4)$ and $w = (w_1,w_2,w_3,w_4)$, be any two arbitrary points. It then follows from the definition of a convex set [38], that

$$\lambda v + (1-\lambda)w \in [0,u_{max}]^4, \text{ for all } \lambda \in [0,u_{max}].$$

Consequently, $\lambda v + (1-\lambda)w \in \mathcal{U}$, implying the convexity of $\mathcal{U}$.

(ii) This property is verified by adopting the ideas of the previous authors [37,39]. Obviously, $f_0(t,x,u)$ in (10) can be written as

$$f_0(t,x,u) = f_1(t,x) + f_2(t,x)u,$$

where

$$f_1(t,x) = \begin{pmatrix} \Lambda - \frac{(\beta_1E+\beta_2I+\beta_3A)S}{N} - \frac{\beta_4BS}{N} - dS \\ \frac{(\beta_1E+\beta_2I+\beta_3A)S}{N} + \frac{\beta_4BS}{N} - (\delta+d)E \\ (1-\tau)\delta E - (d+d_1+\gamma_1)I \\ \tau\delta E - (d+\gamma_2)A \\ \gamma_1 I + \gamma_2 A - dR \\ \psi_1 E + \psi_2 I + \psi_3 A - \phi B \end{pmatrix}$$

and

$$f_2(t,x) = \begin{pmatrix} \frac{(\beta_1E+\beta_2I+\beta_3A)S}{N} + \frac{\beta_4BS}{N} & \frac{\beta_4BS}{N} & 0 & 0 \\ -\frac{(\beta_1E+\beta_2I+\beta_3A)S}{N} - \frac{\beta_4BS}{N} & -\frac{\beta_4BS}{N} & 0 & 0 \\ 0 & 0 & 0 & 0 \\ 0 & 0 & 0 & 0 \\ 0 & 0 & 0 & 0 \\ 0 & 0 & -(\psi_1E+\psi_2I+\psi_3A) & -B \end{pmatrix}.$$

Hence,

$$\|f_0(t,x,u)\| \le \|f_1(t,x)\| + \|f_2(t,x)\|\|u\| \le b_1 + b_2\|u\|,$$

where b_1 and b_2 are positive constants given as

$$b_1 = \sqrt{\max\left\{c_1,c_2\right\}\left(\Lambda^2 + \Lambda^2(\psi_1+\psi_2+\psi_3)^2\right)},$$

and

$$b_2 = \sqrt{\max\left\{d_1,d_2\right\}\left(\Lambda^2 + \Lambda^2(\psi_1+\psi_2+\psi_3)^2\right)},$$

with

$$c_0 = d^2 + \beta_3(2\beta_1+2\beta_2+\beta_3) + \left(\beta_1+\beta_2\right)^2 + (1-2\tau+2\tau^2)\delta^2 + \left(\gamma_1+\gamma_2\right)^2 + \psi_3(2\psi_1+2\psi_2+\psi_3) + (\psi_1+\psi_2)^2,$$
$$c_1 = \frac{c_0}{d^2},$$
$$c_2 = \frac{2\beta_4(\beta_1\phi+\beta_2\phi+\beta_3\phi) + \beta_4^2(\psi_1+\psi_2+\psi_3)}{d^2\phi^2(\psi_1+\psi_2+\psi_3)},$$
$$d_1 = \frac{2\beta_3(2\beta_1+2\beta_2+\beta_3) + 2(\beta_1+\beta_2)^2 + (\psi_1+\psi_3)^2 + \psi_2(2\psi_1+\psi_2+2\psi_3)}{d^2},$$
$$d_2 = \frac{4\beta_4\phi(\beta_1+\beta_2+\beta_3) + (1+4\beta_4^2)(\psi_1+\psi_2+\psi_3)}{d^2\phi^2(\psi_1+\psi_2+\psi_3)}.$$

(iii) First note that the objective functional $\mathcal{J}$ in (9) has an integrand of the Lagrangian form defined as

$$\mathcal{L}(t,x,u) = A_1E + A_2I + A_3A + A_4B + \frac{1}{2}\sum_{i=1}^{4} D_iu_i^2. \quad (11)$$

Let $v = (v_1,v_2,v_3,v_4) \in \mathcal{U}$, $w = (w_1.w_2,w_3,w_4) \in \mathcal{U}$ and $\lambda \in [0,u_{max}]$, then it suffices to prove that

$$\mathcal{L}(t,x,(1-\lambda)v + \lambda w) \le (1-\lambda)\mathcal{L}(t,x,v) + \lambda\mathcal{L}(t,x,w). \quad (12)$$

From (11),

$$\mathcal{L}(t,x,(1-\lambda)v+\lambda w) = A_1E+A_2I+A_3A+A_4B+\frac{1}{2}\sum_{i=1}^{4}\left[D_i((1-\lambda)v_i + \lambda w_i)^2\right], \quad (13)$$

and

$$(1-\lambda)\mathcal{L}(t,x,v)+\lambda\mathcal{L}(t,x,w) = A_1E+A_2I+A_3A+A_4B+\frac{1}{2}(1-\lambda)\sum_{i=1}^{4}D_iv_i^2+\frac{1}{2}\lambda\sum_{i=1}^{4}D_iw_i^2. \tag{14}$$

Applying the inequality (12) to the results in (13) and (14) leads to

$$\mathcal{L}(t,x,(1-\lambda)v+\lambda w)-((1-\lambda)\mathcal{L}(t,x,v)+\lambda\mathcal{L}(t,x,w)) = \tfrac{1}{2}(\lambda^2-\lambda)\textstyle\sum_{i=1}^{4}D_i(v_i-w_i)^2\le 0, \text{ since } \lambda\in[0,u_{max}],$$

implying that the integrand $\mathcal{L}(t,x,u)$ of the objective functional $\mathcal{J}$ is convex.

(iv) Lastly, the fourth property is verified as follows:

$$\begin{aligned}\mathcal{L}(t,x,u) &= A_1E+A_2I+A_3A+A_4B+\frac{1}{2}\sum_{i=1}^{4}D_iu_i^2,\\ &\ge \frac{1}{2}\sum_{i=1}^{4}D_iu_i^2,\\ &\ge a_0\left(|u_1|^2+|u_2|^2+|u_3|^2+|u_4|^2\right)^{\frac{a_2}{2}}-a_1,\end{aligned}$$

where $a_0=\frac{1}{2}\max\{D_1,D_2,D_3,D_4\}$, $a_1>0$ and $a_2=2$. □

Characterization of the optimal controls

Pontryagin's maximum principle (PMP) provides the necessary conditions that an optimal control quadruple must satisfy. This principle converts the optimal control problem consisting of the non-autonomous system (6) and the objective functional $\mathcal{J}$ in (7) into an issue of minimizing pointwise a Hamiltonian, denoted as $\mathcal{H}$, with respect to controls $u=(u_1,u_2,u_3,u_4)$. First, the Hamiltonian $\mathcal{H}$ associated with the optimal control problem is formulated as

$$\begin{aligned}\mathcal{H} &= A_1E+A_2I+A_3A+A_4B+\frac{1}{2}\left(D_1u_1^2+D_2u_2^2+D_3u_3^2+D_4u_4^2\right)\\ &+\lambda_1\left[\Lambda-(1-u_1)\left(\beta_1E+\beta_2I+\beta_3A\right)\frac{S}{N}-(1-u_1-u_2)\beta_4B\frac{S}{N}-dS\right]\\ &+\lambda_2\left[(1-u_1)\left(\beta_1E+\beta_2I+\beta_3A\right)\frac{S}{N}+(1-u_1-u_2)\beta_4B\frac{S}{N}-(\delta+d)E\right]\\ &+\lambda_3\left[(1-\tau)\delta E-(d+d_1+\gamma_1)I\right]\\ &+\lambda_4\left[\tau\delta E-(d+\gamma_2)A\right]\\ &+\lambda_5\left[\gamma_1I+\gamma_2A-dR\right]\\ &+\lambda_6\left[(1-u_3)\psi_1E+(1-u_3)\psi_2I+(1-u_3)\psi_3A-(u_4+\phi)B\right],\end{aligned} \tag{15}$$

where λ_i (with $i=1,2,\dots,6$) are the adjoint variables corresponding to the state variables S, E, I, A, R and B respectively.

Theorem 2. *If $u^*=(u_i^*)$, $i=1,\dots,4$ is an optimal control quadruple and S^*, E^*, I^*, A^*, R^*, B^* are the solutions of the corresponding state system (6) that minimizes $\mathcal{J}(u^*)$ over the control set $\mathcal{U}$ defined by (8), then there exist adjoint variables λ_i $(i=1,2,\dots,6)$ satisfying*

$$\begin{aligned}\frac{d\lambda_1}{dt} &= (\lambda_1-\lambda_2)\left[(1-u_1)\left(\beta_1E^*+\beta_2I^*+\beta_3A^*\right)\right]\frac{(E^*+I^*+A^*+R^*)}{N^2}\\ &+(\lambda_1-\lambda_2)(1-u_1-u_2)\beta_4B^*\frac{(E^*+I^*+A^*+R^*)}{N^2}+\lambda_1d,\\ \frac{d\lambda_2}{dt} &= -A_1+(\lambda_1-\lambda_2)(1-u_1)S^*\left[\frac{(S^*+I^*+A^*+R^*)\beta_1-(\beta_2I^*+\beta_3A^*)}{N^2}\right]\\ &+(\lambda_2-\lambda_1)(1-u_1-u_2)\beta_4B^*\frac{S^*}{N^2}+(\delta+d)\lambda_2-\lambda_2(1-\tau)\delta\lambda_3-\tau\delta\lambda_4\\ &-(1-u_3)\psi_1\lambda_6,\\ \frac{d\lambda_3}{dt} &= -A_2+(\lambda_1-\lambda_2)(1-u_1)S^*\left[\frac{(S^*+E^*+A^*+R^*)\beta_2-(\beta_1E^*+\beta_3A^*)}{N^2}\right]\\ &+(\lambda_2-\lambda_1)(1-u_1-u_2)\beta_4B^*\frac{S^*}{N^2}+(\delta+d_1+\gamma_1)\lambda_3-\gamma_1\lambda_5-(1-u_3)\psi_2\lambda_6,\end{aligned} \tag{16}$$

$$\begin{aligned}\frac{d\lambda_4}{dt} &= -A_3+(\lambda_1-\lambda_2)(1-u_1)S^*\left[\frac{(S^*+E^*+I^*+R^*)\beta_3-(\beta_1E^*+\beta_2I^*)}{N^2}\right]\\ &+(\lambda_2-\lambda_1)(1-u_1-u_2)\beta_4B^*\frac{S^*}{N^2}+(d_1+\gamma_2)\lambda_4-\gamma_2\lambda_5-(1-u_3)\psi_3\lambda_6,\\ \frac{d\lambda_5}{dt} &= (\lambda_2-\lambda_1)(1-u_1)\left(\beta_1E^*+\beta_2I^*+\beta_3A^*\right)\frac{S^*}{N^2}\\ &+(\lambda_2-\lambda_1)(1-u_1-u_2)\beta_4\frac{S^*}{N^2}+\lambda_5d,\\ \frac{d\lambda_6}{dt} &= -A_4+(\lambda_1-\lambda_2)(1-u_1-u_2)\beta_4\frac{S^*}{N}+(u_4+\phi)\lambda_6d.\end{aligned}$$

with transversality conditions

$$\lambda_i(T)=0, \quad \text{for } i=1,2,\dots,6 \tag{17}$$

and

$$\begin{cases}u_1^*(t)=\min\left\{\max\left\{0,\dfrac{(\lambda_2-\lambda_1)(\beta_1E^*+\beta_2I^*+\beta_3A^*+\beta_4B^*)S}{D_1N}\right\},u_{1_{max}}\right\},\\ u_2^*(t)=\min\left\{\max\left\{0,\dfrac{(\lambda_2-\lambda_1)\beta_4B^*S^*}{D_2N}\right\},u_{2_{max}}\right\},\\ u_3^*(t)=\min\left\{\max\left\{0,\dfrac{\lambda_6(\psi_1E^*+\psi_2I^*+\psi_3A^*)}{D_3}\right\},u_{3_{max}}\right\},\\ u_4^*(t)=\min\left\{\max\left\{0,\dfrac{\phi B^*\lambda_6}{D_4}\right\},u_{4_{\max}}\right\}.\end{cases} \tag{18}$$

Proof. The form of the adjoint system and the transversality conditions associated with this optimal control problem follows the widely used standard results obtained from work done by Pontryagin et al. [40]. For this purpose, we partially differentiate the formulated Hamiltonian function (15) with respect to S, E, I, A, R and B as follows;

$$\begin{cases}\frac{d\lambda_1}{dt}=-\frac{\partial\mathcal{H}}{\partial S}, & \lambda_1(T)=0,\\ \frac{d\lambda_2}{dt}=-\frac{\partial\mathcal{H}}{\partial E}, & \lambda_2(T)=0,\\ \frac{d\lambda_3}{dt}=-\frac{\partial\mathcal{H}}{\partial I}, & \lambda_3(T)=0,\\ \frac{d\lambda_4}{dt}=-\frac{\partial\mathcal{H}}{\partial A}, & \lambda_4(T)=0,\\ \frac{d\lambda_5}{dt}=-\frac{\partial\mathcal{H}}{\partial R}, & \lambda_5(T)=0,\\ \frac{d\lambda_4}{dt}=-\frac{\partial\mathcal{H}}{\partial B}, & \lambda_6(T)=0.\end{cases} \tag{19}$$

Finally, to obtain the desired results for the characterizations of the optimal control, we need to partially differentiate the Hamiltonian function (15) with respect to the four time-dependent control functions (u_1,u_2,u_3,u_4), thus, further, the optimal control characterization in (18) is obtained by solving

$$\frac{\partial\mathcal{H}}{\partial u_i}=0, \qquad \text{for } u_i^* \qquad (\text{where } i=1,2,3,4).$$

Lastly, it follows from standard control arguments involving bounds on the control that

$$u_i^*=\begin{cases}0 & \text{if } \theta_i^*\le 0,\\ \theta_i^* & \text{if } 0\le\theta_i^*\le u_{i\max},\\ u_{i\max} & \text{if } \theta_i^*\ge u_{i\max},\end{cases}$$

where $i=1,2,3,4$ and with

$$\theta_1=\frac{(\lambda_2-\lambda_1)(\beta_1E+\beta_2I+\beta_3A+\beta_4B)S}{D_1N},$$

$$\theta_2=\frac{(\lambda_2-\lambda_1)\beta_4BS}{D_2N},$$

$$\theta_3=\frac{\lambda_6(\psi_1E+\psi_2I+\psi_3A)}{D_3},$$

$$\theta_4=\frac{\phi B\lambda_6}{D_4}. \quad \square$$

Numerical simulation and cost-effectiveness analysis

Numerical simulation

Numerical simulations are vital in dynamical modelling; they give the proposed model's pictorial view to the theoretical analysis. Hence, we provide the numerical outcomes of our study by simulating 14 possible strategic combinations of the control measures. This is done by simulating the constraint system (6) froward in time and the adjoint system (15) backward in time until convergence is reached. The model parameters can be found in [20], but restated here for easy reference see Table 1. This simulation procedure is popularly known as fourth-order Runge–Kutta forward–backward sweep simulations. The 14 possible strategic combination strategies are divided into four scenarios, thus, the implementation of single control (Scenario A), the use of dual controls (Scenario B), the performance of triple controls (Scenario C) and lastly, the implementation of quadruplet control measures (Scenario D). Iterated below as

- ♠ Scenario A (implementation of single control)
  - ✠ Strategy 1: practising physical or social distancing protocols only $(u_1 \neq 0, u_2 = u_3 = u_4 = 0)$.
  - ✠ Strategy 2: practising personal hygiene by cleaning contaminated surfaces with alcohol based detergents only $(u_1 = 0, u_2 \neq 0, u_3 = u_4 = 0)$.
  - ✠ Strategy 3: practising proper and safety measures by exposed, asymptomatic infected and symptomatic infected individuals only $(u_1 = 0, u_2 = 0, u_3 \neq 0, u_4 = 0)$.
  - ✠ Strategy 4: Fumigating schools in all levels of education, sports facilities, commercial areas and religious worship centres only $(u_1 = 0, u_2 = 0, u_3 = 0, u_4 \neq 0)$.
- ♠ Scenario B (the use of double controls)
  - ✠ Strategy 5: practising physical or social distancing protocols + practising personal hygiene by cleaning contaminated surfaces with alcohol based detergents $(u_1, u_2 \neq 0, u_3 = u_4 = 0)$.
  - ✠ Strategy 6: practising physical or social distancing protocols + practising proper and safety measures by exposed, asymptomatic infected and symptomatic infected individuals $(u_1, u_3 \neq 0, u_2 = u_4 = 0)$.
  - ✠ Strategy 7: practising physical or social distancing protocols + fumigating schools in all levels of education, sports facilities, commercial areas and religious worship centres $(u_1, u_4 \neq 0, u_2 = 0, u_3 = 0)$.
  - ✠ Strategy 8: practising personal hygiene by cleaning contaminated surfaces with alcohol based detergents + practising proper and safety measures by exposed, asymptomatic infected and symptomatic infected individuals $(u_2, u_3 \neq 0, u_1 = 0, u_4 = 0)$.
  - ✠ Strategy 9: practising personal hygiene by cleaning contaminated surfaces with alcohol based detergents + fumigating schools in all levels of education, sports facilities, commercial areas and religious worship centres $(u_2, u_4 \neq 0, u_1 = 0, u_3 = 0)$.
  - ✠ Strategy 10: practising proper and safety measures by exposed, asymptomatic infected and symptomatic infected individuals + fumigating schools in all levels of education, sports facilities, commercial areas and religious worship centres $(u_3, u_4 \neq 0, u_1 = 0, u_2 = 0)$.
- ♠ Scenario C (the use of triple controls)
  - ✠ Strategy 11: practising physical or social distancing protocols + practising personal hygiene by cleaning contaminated surfaces with alcohol based detergents + practising proper and safety measures by exposed, asymptomatic infected and symptomatic infected individuals $(u_1, u_2, u_3 \neq 0, u_4 = 0)$.
  - ✠ Strategy 12: practising physical or social distancing protocols + practising personal hygiene by cleaning contaminated surfaces with alcohol based detergents + fumigating schools in all levels of education, sports facilities, commercial areas and religious worship centres $(u_1, u_2, u_4 \neq 0, u_3 = 0)$.
  - ✠ Strategy 13: practising personal hygiene by cleaning contaminated surfaces with alcohol based detergents + practising proper and safety measures by exposed, asymptomatic infected and symptomatic infected individuals + fumigating schools in all levels of education, sports facilities, commercial areas and religious worship centres $(u_2, u_3, u_4 \neq 0, u_1 = 0)$.
- ♠ Scenario D (implementation of quadruplet)
  - ✠ Strategy 14: practising physical or social distancing protocols + practising personal hygiene by cleaning contaminated surfaces with alcohol based detergents + practising proper and safety measures by exposed, asymptomatic infected and symptomatic infected individuals + fumigating schools in all levels of education, sports facilities, commercial areas and religious worship centres $(u_1, u_2, u_3, u_4 \neq 0)$.

Scenario A: use of single control

In Fig. 1(a), we noticed that strategy 1 has the highest number of exposed and asymptomatic averted individuals, followed by strategy 4, strategy 3, and then strategy 1. Likewise, in Fig. 1(b) we noticed that the dynamical importance of the strategy is of equal usefulness on the number of symptomatic individuals. In Fig. 1(c), we saw that the strategy with the highest number of virus removal from the environment is strategy 4, with strategy 2 having the lowest viral removal effect. In Fig. 1(d), the control profiles suggest that the optimal strategy for scenario A should be implemented on the same control level. In other words, it indicates that if the controls are kept on the same level, it can help reduce the infection when one considers the optimal strategies for scenario A. Fig. 1(e) shows the infection averted ratio of the various control strategies. It shows that strategy 2 (practising personal hygiene by cleaning contaminated surfaces with alcohol-based detergents only), is the most effective strategy if health officials stick to scenario A only in controlling COVID-19 in the Kingdom of Saudi Arabia. Fig. 1(f) shows the average cost-effectiveness ratio, which also supports that strategy 1 is the most effective and cost-saving strategy in scenario A. The mathematical extraction of the infection averted ratio and the average cost-effectiveness ratio can be found in Section h where we validate the claim on Figs. 1(e) and 1(f) respectively.

Scenario B: use of double controls

In Figs. 2(a)–2(d), we carried out numerical simulations with the notion that an individual may apply two of the suggested controls simultaneously. We noticed in Fig. 2(a) that strategy 5 has the highest number of exposed and asymptomatic averted individuals, in the long run, followed by strategy 6, strategy 7, strategy 9, strategy 10 and then strategy 8. Likewise, in Fig. 2(b) we noticed that the dynamical importance of the strategy is of equal usefulness on the number of symptomatic individuals. In Fig. 2(c), we saw that the strategy with the highest number of virus removal from the environment is strategy 7 and 9, with strategy 8 having the most minimal viral removal effect. In Fig. 2(d), the control profiles suggest that the optimal strategy for scenario B should be implemented on a control level of 0.75 for each control term in strategy 5 and 8 for the entire simulation period. For the control strategy 9 in Fig. 2(d), we noticed that the control terms

Table 1
Model's parameter descriptions and values.

Parameter	Definition	Value	Source
Λ	Recruitment rate	$d \times N(0)$	[20]
d	Natural mortality rate	$\frac{1}{74.87\times365}$	[20]
β_1	Contact rate among exposed and susceptible	0.1233	[20]
β_2	Contact rate among infected (symptomatic) and susceptible	0.0542	[20]
β_3	Contact rate among infected (asymptomatic) and susceptible	0.0020	[20]
β_4	Contact rate among environment and susceptible	0.1101	[20]
δ	Incubation period	0.1980	[20]
τ	fraction that transient to A	0.3085	[20]
d_1	Natural death rate due to Infection at I	0.0104	[20]
γ_1	Recovery from I	0.3680	[20]
γ_2	Recovery from A	0.2945	[20]
ψ_1	Virus contribution due to E to B	0.2574	[20]
ψ_2	Virus contribution due to I to B	0.2798	[20]
ψ_3	Virus contribution due to A to B	0.1584	[20]
ϕ	Virus removal from environment	0.3820	[20]

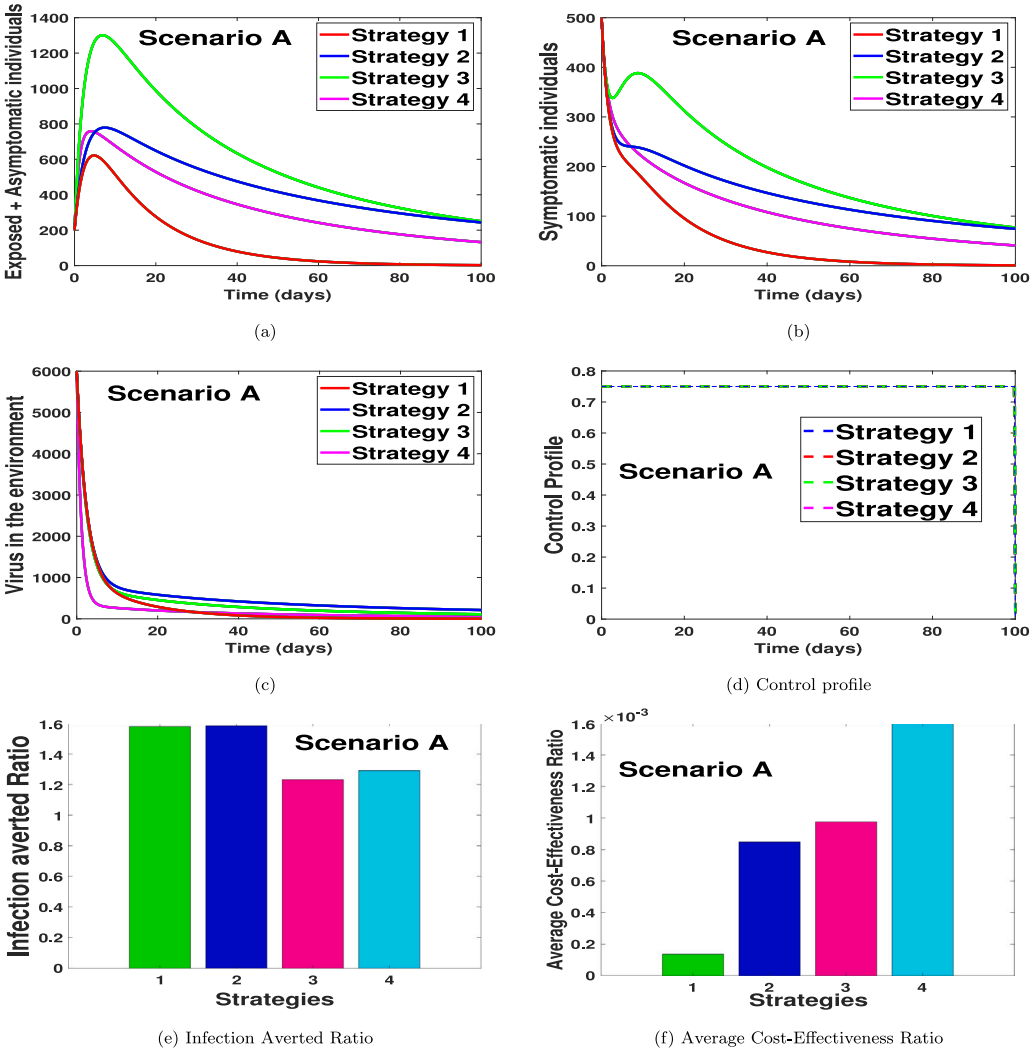

Fig. 1. Single control strategy.

in strategy 9, should be kept at 0.75 for 95 days and then reduced to 0.5 for each of the control terms for the rest of the simulation time. The control profile for strategy 10 shows that each control term should be kept for 0.75 for 92 days and then reduced to 0.5 for the rest of the simulation period. The control profile for strategy 6 shows that, with the combined effort of the two controls, the strategy control level should be kept at 1.5 for 65 days and then gradually reduced to 0.98 for the entire simulation time. We also noticed in Fig. 2(d) that the control profile of strategy 7 shows that the control level for the two controls in strategy 7 should be kept at 1.5, thus 0.75 each for 41 days and then gradually reduced to 1 for the entire simulation time. Fig. 2(e) shows the infection averted ratio of the various control strategies. It shows that strategy 5 is the most effective when one uses the infection averted ratio (IAR). Fig. 2(f) shows the average cost-effectiveness ratio, which indicates that strategy 6 is the most effective and cost-saving strategy in scenario B. The mathematical extraction of the infection averted ratio

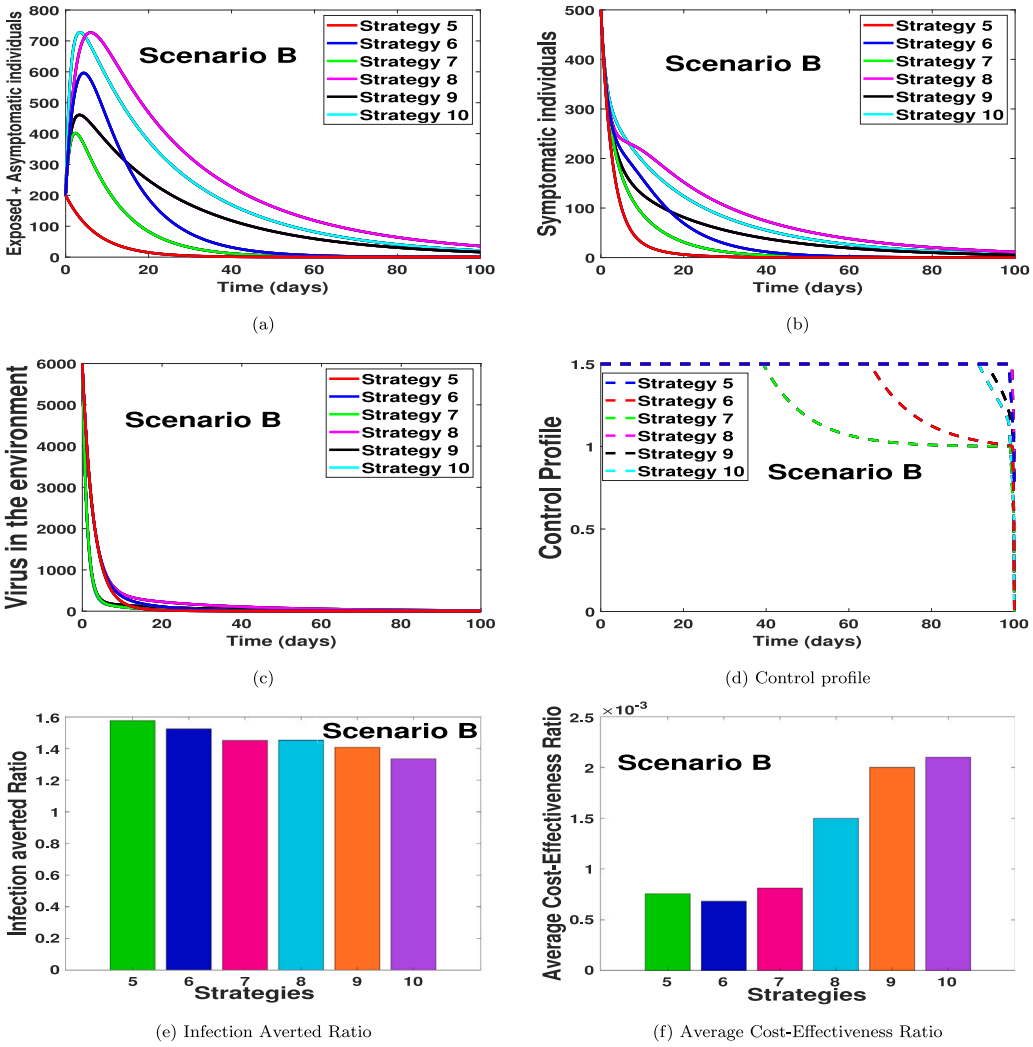

Fig. 2. Double control strategies.

and the average cost-effectiveness ratio can be found in Section h where we validate the claim on Figs. 2(e) and 2(f) respectively.

Scenario C: use of triple controls

In Figs. 3(a)–3(d), we carried out numerical simulations with the notion that an individual may apply three of the suggested controls simultaneously. We noticed in Fig. 3(a) that strategy 11 has the highest number of exposed and asymptomatic averted individuals, in the long run, followed by strategy 12 and then strategy 13. Likewise, in Fig. 3(b) we noticed that the dynamical importance of the strategy is of equal usefulness on the number of symptomatic individuals. In Fig. 3(c), we noticed that the strategy with the highest number of virus removal from the environment is strategy 13 and 12, with strategy 11 having the most minimum virus removal effect. In Fig. 3(d), the control profiles suggest that the optimal strategies for scenario C should be implemented on a control level of 0.75 for each control term in strategy 11, for 30 days and then reduced to 0.60 for the entire simulation period. For the control strategy 12 in Fig. 3(d), we noticed that the control terms in strategy 12 should be kept at 0.7 for 18 days and then reduced to 0.5 for each of the control terms for the rest of the simulation time. The control profile for strategy 13 shows that each control term should be kept for 0.75 for 70 days and then reduced to 0.47 for the rest of the simulation period. Fig. 3(e) shows the infection averted ratio (IAR) of the various control strategies. The IAR shows that strategy 11 is the most effective. Fig. 3(f) shows the average cost-effectiveness ratio (ACER), which indicates that strategy 12 is the most effective and cost-saving strategy in scenario C. The mathematical extraction of the infection averted ratio and the average cost-effectiveness ratio can be found in Section h, where we validate the claim on Figs. 3(e) and 3(f) respectively.

Scenario D: use of quadruplet controls

In Figs. 4(a)–5(a), we carried out numerical simulations with the notion that an individual may apply all of the suggested controls simultaneously. We noticed in Fig. 4(a) that the number of exposed and asymptomatic individuals drastically reduces when the four controls are applied simultaneously. Fig. 4(b) shows that the disease in the symptomatic individuals can be eliminated within 21 days when one chooses to implement all the controls simultaneously. Fig. 4(c) shows that the virus in the environment can be eliminated within 10 days when one chooses to implement all the controls simultaneously. In Fig. 5(a) we showed the dynamical changes of each control considered in this work. We noticed that, in the pool of the four controls, control u_1 (practising physical or social distancing protocols) and control u_2 (practising personal hygiene by cleaning contaminated surfaces with alcohol-based detergents) should be applied at a constant level throughout, with much effort placed on control u_1 for 98 days. For the control u_3 in Fig. 5(a), we noticed that the control should be kept at 0.75 for 25 days and then gradually reduced to 0.29 for the rest of the simulation time. The control profile for control u_4 shows that the control term

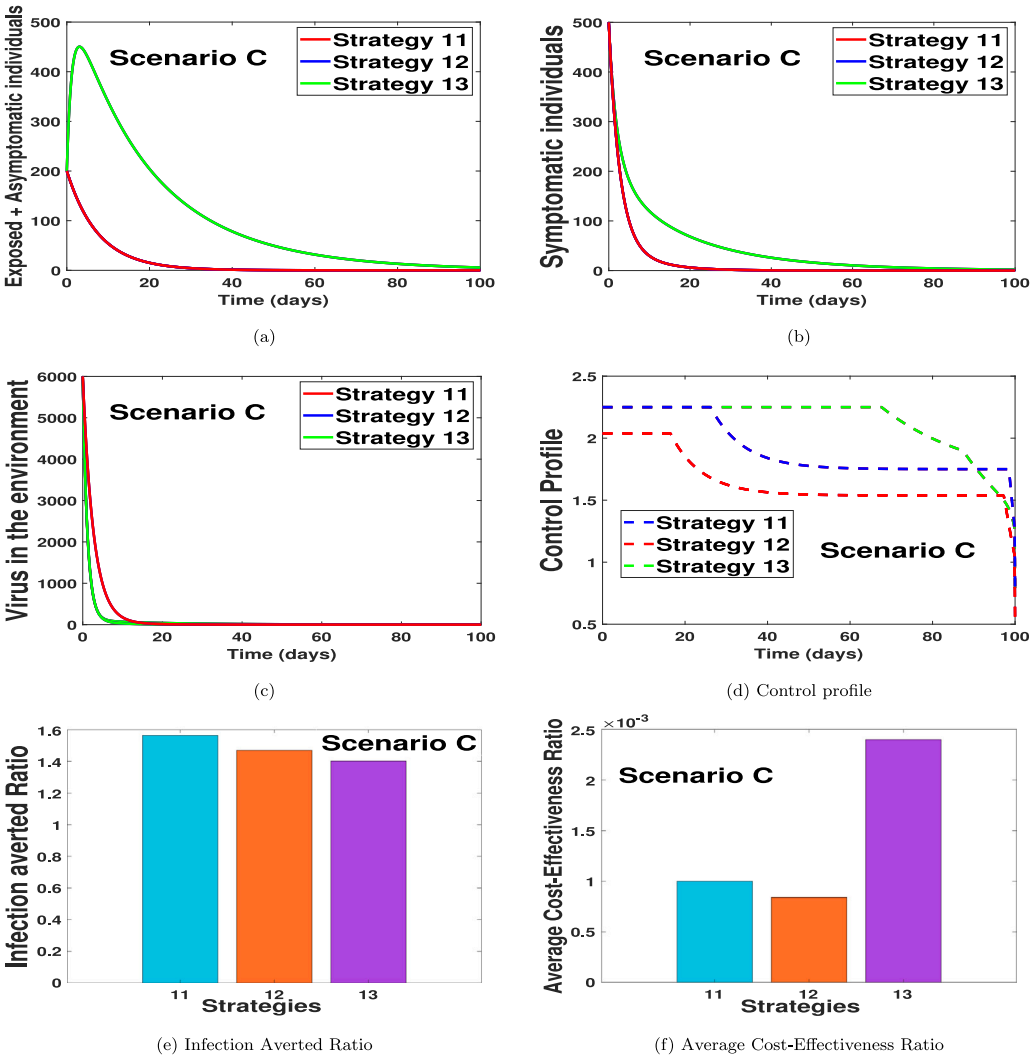

Fig. 3. Implementation of quadruplet controls.

should be kept for 0.75 for 18 days and then gradually reduced to 0.29 for the rest of the simulation period. Finally, Fig. 5(b) shows the efficacies plot for the number of exposed, asymptomatic, symptomatic individuals and the number of viruses removed from the environment, respectively, when one uses all the proposed control simultaneously. We noticed from the efficacies plot that the controls are more efficient on the number of viral removed from the environment, followed by the number of symptomatic individuals, asymptomatic individuals, and exposed individuals. The efficacy plots are obtained from using the following functions:

$$E_E = \frac{E(0)-E^*(t)}{E(0)}, E_I = \frac{I(0)-I^*(t)}{I(0)}, E_A = \frac{A(0)-A^*(t)}{A(0)},$$
$$E_B = \frac{B(0)-B^*(t)}{B(0)}$$

where $E(0), I(0), A(0), B(0)$ are the initial data and $E^*(t), I^*(t), A^*(t), B^*(t)$ are the function relating to the "optimal states associated" with the controls [41]. Fig. 5(b) shows that the controls attain 100% efficacy on the disease induced compartment after 39 days.

Cost-effectiveness analysis

Given the four different scenarios considered for the implementation of optimal control problem in Section h, cost-effectiveness analysis is employed to decide on the most cost-effective control intervention strategy from other strategies for each of scenarios A–D, under investigation. To implement the cost-effectiveness analysis, we use three approaches. These are: infection averted ratio (IAR) [26], average cost-effectiveness ratio (ACER) and incremental cost-effectiveness ratio (ICER) [26,41,42]. Definitions of the three approaches are given as follows:

Infection averted ratio (IAR)

Infection averted ratio (IAR) can be expressed as

$$\text{IAR} = \frac{\text{Number of infections averted}}{\text{Number of individuals recovered from the infection}},$$

where the number of infections averted represents the difference between the total number of infected individuals without any control implementation and the total number of infected individuals with control throughout the simulation, a control strategy with the highest IAR value is considered as the most cost-effective [26,35,42].

Average cost-effectiveness ratio (ACER)

Average cost-effectiveness ratio (ACER) is stated as

$$\text{ACER} = \frac{\text{Total cost incurred on the implementation of a particular intervention strategy}}{\text{Total number of infections averted by the intervention strategy}}.$$

The total cost incurred on implementing a particular intervention strategy is estimated from

$$C(u) = \frac{1}{2}\int_0^T \sum_{i=1}^{4} D_i u_i^2 dt. \tag{20}$$

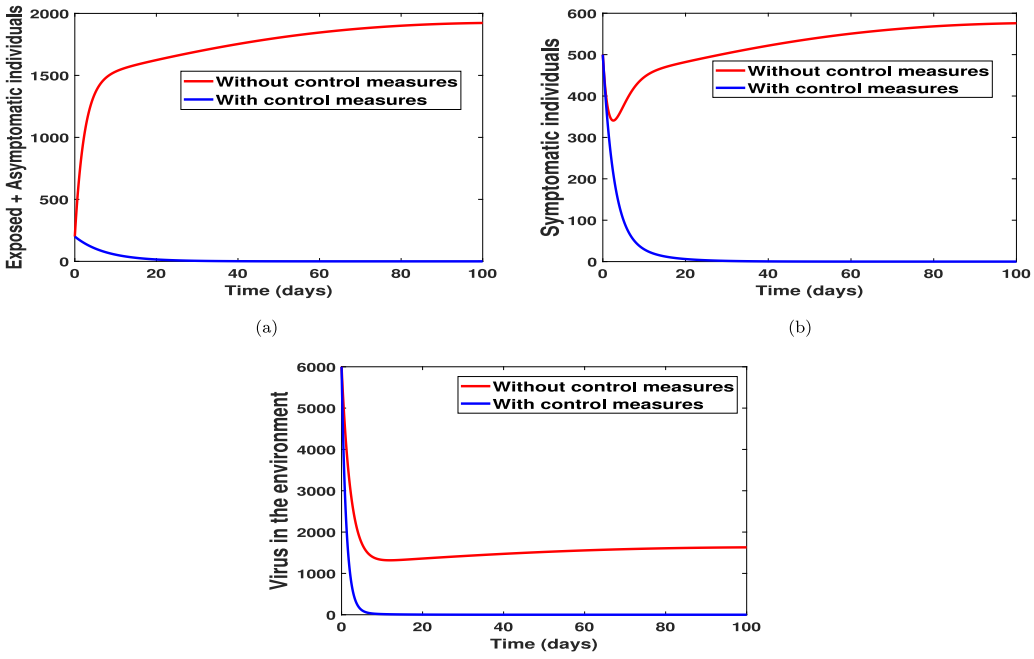

Fig. 4. With and without control strategies.

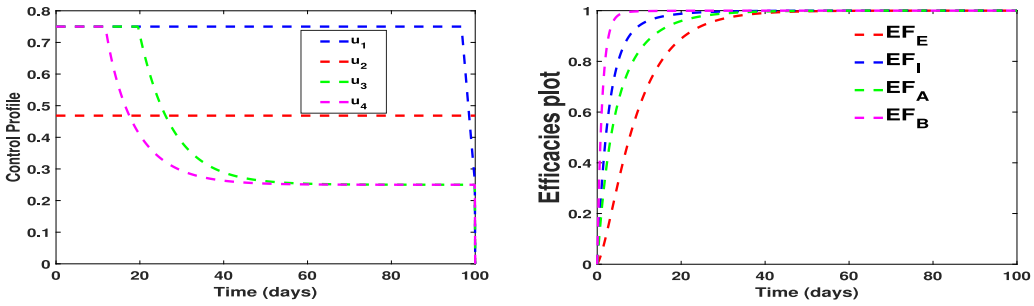

Fig. 5. With and without control strategies.

Incremental cost-effectiveness ratio (ICER)

Usually, the incremental cost-effectiveness ratio (ICER) measures the changes between the costs and health benefits of any two different intervention strategies competing for the same limited resources. Considering strategies p and q as two competing control intervention strategies, then ICER is stated as

$$\text{ICER} = \frac{\text{Change in total costs in strategies p and q}}{\text{Change in control benefits in strategies p and q}}.$$

ICER numerator includes the differences in disease averted costs, costs of prevented cases, intervention costs, among others. While the denominator of ICER accounts for the differences in health outcome, including the total number of infections averted or the total number of susceptibility cases prevented.

Scenario A: use of single control

Owing to the simulated results of the optimality system under scenario A (when only one control is implemented with considerations of strategies 1–4) as shown in Fig. 1, we calculate IAR, ACER and ICER for each of the four control strategies.

For IAR, the fourth column of Table 2 summarizes the calculated values for the implemented strategies. Accordingly, strategy 2 (practising personal hygiene by cleaning contaminated surfaces with alcohol-based detergents only) has the highest IAR value, followed by strategy 1 (practising physical or social distancing protocol only), strategy 4 (fumigating schools in all levels of education, sports facilities and commercial areas such as markets and public toilet facilities only), and lastly strategy 3 (practising proper and safety measures by the exposed, asymptomatic infected and symptomatic infected individuals only). Consequently, the most cost-effective strategy according to this cost-effectiveness analysis approach is strategy 2. The next most cost-effective strategy is strategy 1, followed by strategy 4, then strategy 3.

According to the ACER cost-effectiveness analysis method, strategy 4 has the highest ACER value, followed by strategy 3, strategy 2 and strategy 1 as shown in the fifth column of Table 2. Therefore, the cost-effectiveness of the four strategies implemented, ranging from the most cost-effective to the least cost-effective strategy, is given as strategy 1, strategy 2, strategy 3, and strategy 4.

Next, ICER values are computed for the four control intervention strategies under scenario A to further affirm the most economical strategy among them. Based on the results obtained for the numerical

Table 2
Incremental cost-effectiveness ratio for scenario A.

Strategy	Infection averted	Cost	IAR	ACER	ICER
Strategy 3: $u_3(t)$	1.4423×10^6	1.4063×10^3	1.2325	9.7498×10^{-4}	9.7498×10^{-4}
Strategy 2: $u_2(t)$	1.6603×10^6	1.4077×10^3	1.5835	8.4784×10^{-4}	6.4220×10^{-6}
Strategy 4: $u_4(t)$	1.8000×10^6	2.8098×10^3	1.2914	0.0016	0.0100
Strategy 1: $u_1(t)$,	2.0679×10^6	281.1135	1.5793	1.3594×10^{-4}	−0.0004

Table 3
Incremental cost-effectiveness ratio for scenario A.

Strategy	Infection averted	Cost	IAR	ACER	ICER
Strategy 3: $u_3(t)$	1.4423×10^6	1.4063×10^3	1.2325	9.7498×10^{-4}	9.7504×10^{-4}
Strategy 2: $u_2(t)$	1.6603×10^6	1.4077×10^3	1.5835	8.4784×10^{-4}	6.4220×10^{-6}
Strategy 1: $u_1(t)$,	2.0679×10^6	281.1135	1.5793	1.3594×10^{-4}	−0.0028

simulations of optimal control problem in scenario A (see Fig. 1), strategies 1–4 are ranked according to their increasing order in respect of the total number of COVID-19 infections averted in the community. We have that Strategy 3 averts the least number of the disease infections, followed by Strategy 2, Strategy 4 and Strategy 1 as shown in Table 2.

Thus, ICER is computed for the competing control Strategy 1, Strategy 2, Strategy 3 and Strategy 4 as follows:

$$\text{ICER}(3) = \frac{1.4063 \times 10^3 - 0}{1.4423 \times 10^6 - 0} = 9.7504 \times 10^{-4},$$
$$\text{ICER}(2) = \frac{1.4077 \times 10^3 - 1.4063 \times 10^3}{1.6603 \times 10^6 - 1.4423 \times 10^6} = 6.4220 \times 10^{-6},$$
$$\text{ICER}(4) = \frac{2.8098 \times 10^3 - 1.4077 \times 10^3}{1.8000 \times 10^6 - 1.6603 \times 10^6} = 0.0100,$$
$$\text{ICER}(1) = \frac{281.1135 - 2.8098 \times 10^3}{2.0679 \times 10^6 - 1.8000 \times 10^6} = -0.0004.$$

The computed results (as presented in Table 2) indicate that the ICER value of Strategy 4, ICER(4), is higher than that of Strategy 3. This means that the singular application of control u_4 (fumigating schools in all levels of education, sports facilities and commercial areas such as markets and public toilet facilities) is more costly and less effective than when only control u_3 (practising proper and safety measures by the exposed, asymptomatic infected and symptomatic infected individuals) is applied. Thus, Strategy 4 is eliminated from the list of alternative control strategies.

Then, ICER is further calculated for the competing Strategy 3 with Strategies 1 and 2. The computation is as follows:

$$\text{ICER}(3) = \frac{1.4063 \times 10^3 - 0}{1.4423 \times 10^6 - 0} = 9.7504 \times 10^{-4},$$
$$\text{ICER}(2) = \frac{1.4077 \times 10^3 - 1.4063 \times 10^3}{1.6603 \times 10^6 - 1.4423 \times 10^6} = 6.4220 \times 10^{-6},$$
$$\text{ICER}(1) = \frac{281.1135 - 1.4077 \times 10^3}{2.0679 \times 10^6 - 1.6603 \times 10^6} = -0.0028.$$

The summary of ICER calculations is summarized in Table 3. Looking at Table 3, it is seen that there is a cost-saving of 6.4220×10^{-6} for Strategy 2 over Strategy 3 following the comparison of ICER(2) and ICER(3). The obtained lower ICER for Strategy 2 indicates that Strategy 2 strongly dominates Strategy 3, implying that Strategy 2 has greater effectiveness at cheaper cost when implemented than Strategy 3. Thus, it is better to eliminate Strategy 3 from the control intervention strategies and focus on the alternative control interventions to implement for limited resources preservation. Consequently, Strategy 3 is excluded, and Strategy 2 is further compared with Strategy 1.

We now face the re-calculation of the ICER for Strategies 1 and 2. The calculations are made as follows:

$$\text{ICER}(2) = \frac{1.4077 \times 10^3 - 0}{1.6603 \times 10^6 - 0} = 8.4784 \times 10^{-4},$$
$$\text{ICER}(1) = \frac{281.1135 - 1.4077 \times 10^3}{2.0679 \times 10^6 - 1.6603 \times 10^6} = -0.0028.$$

The results obtained from ICER computations are presented in Table 4. From Table 4, it is shown that ICER(2) is greater than ICER(1). The implication of the lower ICER value obtained for Strategy 1 is that Strategy 2 is strongly dominated, implying that Strategy 2 is more costly and less effective to implement than Strategy 1. Therefore, Strategy 1 (practising physical or social distancing protocol only) is considered the most cost-effective among the four strategies in Scenario A analysed in this work, which confirms the results in Fig. 1(f).

Scenario B: use of double controls

According to the results obtained from the numerical implementation of the optimality system under Scenario B (when only two different controls are implemented with considerations of Strategies 5–10) as illustrated in Fig. 2, we discuss the IAR, ACER and ICER cost analysis techniques for Strategies 5–10 here.

To compare Strategies 5–10 using the IAR cost analysis approach, the computed values for the six control strategies are as presented in the fourth column of Table 5. A look at Table 5 shows that Strategy 5 has the highest IAR. This is followed by Strategy 6, then Strategies 8, 7, 9 and 10. Therefore, it follows that Strategy 5 (which combines practising physical or social distancing protocols with practising personal hygiene by cleaning contaminated surfaces with alcohol-based detergents) is considered most cost-effective among the six strategies in Scenario B as analysed according to the IAR cost analysis technique.

Also, we use the ACER technique to determine the most cost-effective strategy among the various intervention strategies considered in Scenario B. From the results obtained (as shown contained in the fifth column of Table 5), it is clear that Strategy 6 has the least ACER value, followed by Strategies 5, 7, 8, 9 and 10. Hence, Strategy 6 (which combines practising physical or social distancing protocols with practising proper and safety measures by exposed, asymptomatic infected and asymptomatic infected individuals) is the most cost-effective among the set of control strategies considered in Scenario B based on the ACER cost-effective analysis method.

To further affirm the most cost-effective strategy among Strategies 5–10, we implement ICER cost analysis approach on the six intervention strategies. Using the simulated results (as demonstrated in Fig. 2), the six control strategies are ranked from least to most effective according to the number of COVID-19 infections averted as shown in Table 5. So, Strategy 8 averts the least number of infections, followed by Strategy 10, Strategy 9, Strategy 6, Strategy 7 and Strategy 5, averting the most number of infections in the population.

The ICER value for each strategy is computed as follows:

$$\text{ICER}(8) = \frac{2.8104 \times 10^3 - 0}{1.9253 \times 10^6 - 0} = 0.0015,$$
$$\text{ICER}(10) = \frac{4.1019 \times 10^3 - 2.8104 \times 10^3}{1.9809 \times 10^6 - 1.9253 \times 10^6} = 0.0232,$$
$$\text{ICER}(9) = \frac{4.1495 \times 10^3 - 4.1019 \times 10^3}{2.0684 \times 10^6 - 1.9809 \times 10^6} = 5.4400 \times 10^{-4},$$
$$\text{ICER}(6) = \frac{1.3487 \times 10^3 - 4.1495 \times 10^3}{2.1128 \times 10^6 - 2.0684 \times 10^6} = -00631,$$
$$\text{ICER}(7) = \frac{1.7708 \times 10^3 - 1.3487 \times 10^3}{2.1751 \times 10^6 - 2.1128 \times 10^6} = 0.0068,$$

Table 4
Incremental cost-effectiveness ratio for scenario A.

Strategy	Infection averted	Cost	IAR	ACER	ICER
Strategy 2: $u_2(t)$	1.6603×10^6	1.4077×10^3	1.5835	8.4784×10^{-4}	8.4784×10^{-4}
Strategy 1: $u_1(t)$,	2.0679×10^6	281.1135	1.5793	1.3594×10^{-4}	−0.0028

Table 5
Incremental cost-effectiveness ratio for scenario B.

Strategy	Infection averted	Cost	IAR	ACER	ICER
Strategy 8: $u_2(t), u_3(t)$	1.9253×10^6	2.8104×10^3	1.4524	0.0015	0.0015
Strategy 10: $u_3(t), u_4(t)$	1.9809×10^6	4.1019×10^3	1.3350	0.0021	0.0232
Strategy 9: $u_2(t), u_4(t)$	2.0684×10^6	4.1495×10^3	1.4077	0.0020	5.4400×10^{-4}
Strategy 6: $u_1(t), u_3(t)$	2.1128×10^6	1.3487×10^3	1.5239	6.3834×10^{-4}	−0.0631
Strategy 7: $u_1(t), u_4(t)$	2.1751×10^6	1.7708×10^3	1.4506	8.1410×10^{-4}	0.0068
Strategy 5: $u_1(t), u_2(t)$	2.2265×10^6	1.6871×10^3	1.5759	7.5775×10^{-4}	−0.0016

Table 6
Incremental cost-effectiveness ratio for scenario B.

Strategy	Infection averted	Cost	IAR	ACER	ICER
Strategy 8: $u_2(t), u_3(t)$	1.9253×10^6	2.8104×10^3	1.4524	0.0015	0.0015
Strategy 9: $u_2(t), u_4(t)$	2.0684×10^6	4.1495×10^3	1.4077	0.0020	0.0094
Strategy 6: $u_1(t), u_3(t)$	2.1128×10^6	1.3487×10^3	1.5239	6.3834×10^{-4}	−0.0631
Strategy 7: $u_1(t), u_4(t)$	2.1751×10^6	1.7708×10^3	1.4506	8.1410×10^{-4}	0.0068
Strategy 5: $u_1(t), u_2(t)$	2.2265×10^6	1.6871×10^3	1.5759	7.5775×10^{-4}	−0.0016

$$\text{ICER}(5) = \frac{1.6871 \times 10^3 - 1.7708 \times 10^3}{2.2265 \times 10^6 - 2.1751 \times 10^6} = -0.0016.$$

From Table 5, it is observed that there is a cost-saving of \$0.0068 for Strategy 7 over Strategy 10. This follows the comparison of ICER(7) and ICER(10). The indication of the lower ICER value obtained for Strategy 7 is that Strategy 7 strongly dominates Strategy 10. By implication, Strategy 10 is more costly and less effective to implement when compared with Strategy 7. Therefore, it is better to exclude Strategy 10 from the set of alternative intervention strategies. At this point, Strategy 7 is compared with Strategies 5, 6, 8 and 9.

The ICER is computed as

$$\text{ICER}(8) = \frac{2.8104 \times 10^3 - 0}{1.9253 \times 10^6 - 0} = 0.0015,$$
$$\text{ICER}(9) = \frac{4.1495 \times 10^3 - 2.8104 \times 10^3}{2.0684 \times 10^6 - 1.9253 \times 10^6} = 0.0094,$$
$$\text{ICER}(6) = \frac{1.3487 \times 10^3 - 4.1495 \times 10^3}{2.1128 \times 10^6 - 2.0684 \times 10^6} = -00631,$$
$$\text{ICER}(7) = \frac{1.7708 \times 10^3 - 1.3487 \times 10^3}{2.1751 \times 10^6 - 2.1128 \times 10^6} = 0.0068,$$
$$\text{ICER}(5) = \frac{1.6871 \times 10^3 - 1.7708 \times 10^3}{2.2265 \times 10^6 - 2.1751 \times 10^6} = -0.0016.$$

The results obtained are summarized in Table 6. Table 6 shows a cost-saving of \$0.0068 for Strategy 7 over Strategy 9 by comparing ICER(7) and ICER(9). The higher ICER value obtained for Strategy 9 implies that Strategy 9 is strongly dominated, more costly and less effective to implement when compared with Strategy 7. Therefore, Strategy 9 is left out of the list of alternative control interventions to implement for the purpose of preserving the limited resources. We further compare Strategy 7 with Strategies 5, 6 and 8.

The computation of ICER for Strategies 5, 6, 7 and 8 is as follows:

$$\text{ICER}(8) = \frac{2.8104 \times 10^3 - 0}{1.9253 \times 10^6 - 0} = 0.0015,$$
$$\text{ICER}(6) = \frac{1.3487 \times 10^3 - 2.8104 \times 10^3}{2.1128 \times 10^6 - 1.9253 \times 10^6} = -0.0078,$$
$$\text{ICER}(7) = \frac{1.7708 \times 10^3 - 1.3487 \times 10^3}{2.1751 \times 10^6 - 2.1128 \times 10^6} = 0.0068,$$
$$\text{ICER}(5) = \frac{1.6871 \times 10^3 - 1.3487 \times 10^3}{2.2265 \times 10^6 - 2.1128 \times 10^6} = 0.0030.$$

The summary of the results obtained is presented in Table 7.

Looking at Table 7, a comparison of ICER(7) and ICER(8) shows a cost-saving of \$0.0015 for Strategy 8 over Strategy 7. The lower ICER obtained for Strategy 8 is that Strategy 7 is strongly dominated, more costly and less effective to implement than Strategy 8. Thus, it is better to discard Strategy 7 from the list of alternative intervention strategies. At this juncture, Strategy 8 is further compared with Strategies 5 and 6.

The calculation of ICER is given as

$$\text{ICER}(8) = \frac{2.8104 \times 10^3 - 0}{1.9253 \times 10^6 - 0} = 0.0015,$$
$$\text{ICER}(6) = \frac{1.3487 \times 10^3 - 2.8104 \times 10^3}{2.1128 \times 10^6 - 1.9253 \times 10^6} = -0.0078,$$
$$\text{ICER}(5) = \frac{1.6871 \times 10^3 - 1.3487 \times 10^3}{2.2265 \times 10^6 - 2.1128 \times 10^6} = 0.0030.$$

Table 8 summarizes the results obtained from the ICER computations. In Table 8, it is shown that there is a cost-saving of \$0.0015 for Strategy 8 over Strategy 5 following the comparison of ICER(5) with ICER(8). The higher ICER value for Strategy 5 suggests that Strategy 5 is strongly dominated, more costly and less effective to implement than Strategy 8. Hence, Strategy 5 is discarded from the set of alternative intervention strategies. Finally, Strategy 8 is compared with Strategy 6. The ICER is computed as follows:

$$\text{ICER}(8) = \frac{2.8104 \times 10^3 - 0}{1.9253 \times 10^6 - 0} = 0.0015,$$
$$\text{ICER}(6) = \frac{1.3487 \times 10^3 - 2.8104 \times 10^3}{2.1128 \times 10^6 - 1.9253 \times 10^6} = -0.0078.$$

We give the summary of the results in Table 9.

Table 9 reveals that ICER(8) is greater than ICER(6), implying that Strategy 8 is strongly dominated by Strategy 6. This indicates that Strategy 8 is more costly and less effective to implement when compared with Strategy 6. Therefore, Strategy 8 is excluded from the list of alternative intervention strategies. Consequently, Strategy 6 (which combines practising physical or social distancing protocols with practising proper and safety measures by exposed, asymptomatic infected and asymptomatic infected individuals) is considered most cost-effective among the six different control strategies in Scenario B under investigation in this study, which confirms the results in Fig. 2(f).

Scenario C: use of triple controls

This part explores the implementation of IAR, ACER and ICER cost analysis techniques on Strategies 11, 12 and 13 using the results obtained from the numerical simulations of the optimality system under Scenario C as presented in Fig. 3.

Table 7
Incremental cost-effectiveness ratio for scenario B.

Strategy	Infection averted	Cost	IAR	ACER	ICER
Strategy 8: $u_2(t), u_3(t)$	1.9253×10^6	2.8104×10^3	1.4524	0.0015	0.0015
Strategy 6: $u_1(t), u_3(t)$	2.1128×10^6	1.3487×10^3	1.5239	6.3834×10^{-4}	−0.0078
Strategy 7: $u_1(t), u_4(t)$	2.1751×10^6	1.7708×10^3	1.4506	8.1410×10^{-4}	0.0068
Strategy 5: $u_1(t), u_2(t)$	2.2265×10^6	1.6871×10^3	1.5759	7.5775×10^{-4}	−0.0016

Table 8
Incremental cost-effectiveness ratio for scenario B.

Strategy	Infection averted	Cost	IAR	ACER	ICER
Strategy 8: $u_2(t), u_3(t)$	1.9253×10^6	2.8104×10^3	1.4524	0.0015	0.0015
Strategy 6: $u_1(t), u_3(t)$	2.1128×10^6	1.3487×10^3	1.5239	6.3834×10^{-4}	−0.0078
Strategy 5: $u_1(t), u_2(t)$	2.2265×10^6	1.6871×10^3	1.5759	7.5775×10^{-4}	0.0030

Table 9
Incremental cost-effectiveness ratio for scenario B.

Strategy	Infection averted	Cost	IAR	ACER	ICER
Strategy 8: $u_2(t), u_3(t)$	1.9253×10^6	2.8104×10^3	1.4524	0.0015	0.0015
Strategy 6: $u_1(t), u_3(t)$	2.1128×10^6	1.3487×10^3	1.5239	6.3834×10^{-4}	−0.0078

Table 10
Incremental cost-effectiveness ratio for scenario C.

Strategy	Infection averted	Cost	IAR	ACER	ICER
Strategy 13: $u_2(t), u_3(t), u_4(t)$	2.1053×10^6	5.0186×10^3	1.4022	0.0024	0.0024
Strategy 11: $u_1(t), u_2(t), u_3(t)$	2.2265×10^6	2.2464×10^3	1.5641	0.0010	−0.0229
Strategy 12: $u_1(t), u_2(t), u_4(t)$	2.2265×10^6	1.8726×10^3	1.4706	8.4107×10^{-4}	–

To determine the most cost-effective strategy among strategies 11, 12 and 13 using the IAR method, the obtained IAR values for the three strategies are given in the fourth column of Table 10. It is shown that Strategy 11 has the highest IAR value, followed by Strategy 12, then Strategy 13, which has the lowest IAR value. Therefore, based on this cost analysis approach, Strategy 11 (which combines practising physical or social distancing protocols with the efforts of practising personal hygiene by cleaning contaminated surfaces with alcohol-based detergents and practising proper and safety measures by exposed, asymptomatic infected and asymptomatic infected individual) is the most cost-effective control strategy to implement in Scenario C.

Also, the ACER cost analysis approach is employed to determine the most cost-effective strategy among Strategies 11, 12 and 13. To do this, the ACER values obtained for these strategies are as given in the fifth column of Table 10. It is observed that Strategy 12 has the lowest ACER value. The successive strategy with the lowest ACER value is Strategy 11, followed by Strategy 13, which has the highest ACER value. Therefore, according to ACER cost analysis, Strategy 12 is the most cost-effective Strategy to implement in Scenario C.

The cost-effective strategy among Strategies 11, 12 and 13 is considered in Scenario C using ICER and cost-minimizing analysis technique due to the equal number of infection averted by Strategies 11, 12. To implement this technique, the three intervention strategies are ranked in increasing order based on the total number of COVID-19 infections averted.

The calculation of ICER in Table 10 is demonstrated as follows:

$$\text{ICER}(13) = \frac{5.0186 \times 10^3}{2.1053 \times 10^6} = 0.0024,$$

$$\text{ICER}(11) = \frac{2.2464 \times 10^3 - 5.0186 \times 10^3}{2.2265 \times 10^6 - 2.1053 \times 10^6} = -0.0229.$$

Note that, due to the equal number of infection averted by Strategies 11, 12, the ICER is not compared between these strategies. It is shown in Table 10 that ICER(13) is greater than ICER(11). Thus, Strategy 11 strongly dominates Strategy 13, implying that Strategy 11 has greater effectiveness at cheaper cost when implemented than Strategy 13. Therefore, Strategy 13 is eliminated from the list of alternative control strategies. At this point, there is no need to re-compute ICER further for the competing Strategies 11 and 12 because the two strategies avert the same total number of infections. However, the minimization cost technique is used to decide which of the strategies is more cost-effective. It is seen that Strategy 12 requires a lower cost to be implemented compared to Strategy 11. Therefore, Strategy 12 (which combines practising physical or social distancing protocols with the efforts of practising personal hygiene by cleaning contaminated surfaces with alcohol-based detergents and Fumigating schools in all levels of education, sports facilities and commercial areas such as markets and public toilet facilities) is considered the most cost-effective strategy in Scenario C.

Scenario D: implementation of quadruplet

Using the simulated results for the optimality system when Strategy 14 in Scenario D is implemented (see Fig. 4), the cost-effective analysis of this Strategy based on IAR, ACER shown.

Table 11 gives the summary of the results obtained from implementing the IAR and ACER cost analysis techniques.

Determination of the overall most cost-effective strategy

So far, we have been able to obtain the most cost-effective strategy corresponding to each of the four scenarios considered in this study and also noticed from Fig. 4 that using all the controls reduces the disease faster. Hence, it is also essential to determine the most cost-effective strategy from the four most cost-effective strategy corresponding to a particular scenario. Thus, IAR, ACER and ICER cost analysis techniques are implemented for Strategy 1 (from Scenario A), Strategy 6 (from Scenario B), Strategy 12 (from Scenario C) and Strategy 14 (from Scenario D).

To compare Strategies 1, 6, 12 and 14 using IAR cost analysis technique, it is observed in Fig. 6(a) and Table 12 that Strategy 1 has the highest IAR value, followed by Strategy 11, Strategy 6 and Strategy 14. It follows that Strategy 1 (practising physical or social distancing protocols only) is the overall most cost-effective strategy among all the strategies of Scenarios A to D combined as analysed in this work.

Based on the ACER cost analysis technique, and using the results illustrated in Fig. 6(b) and Table 12, it is noted that Strategy 1 has the least ACER value. Strategy 6 is the next strategy with the least

Table 11
Application of optimal controls: scenario D.

Strategy	Infection averted	Cost	IAR	ACER
Strategy 14: $u_1(t), u_2(t), u_3(t), u_4(t)$	2.2265×10^6	2.0437×10^3	1.4662	9.1789×10^{-4}

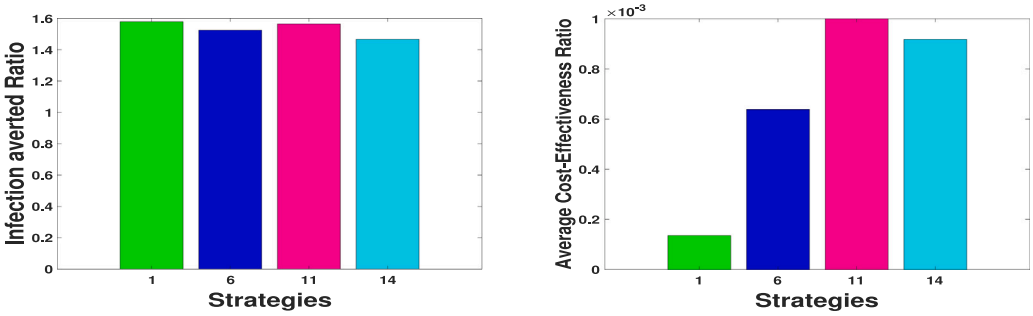

(a) Infection Averted Ratio (b) Average Cost-Effectiveness Ratio

Fig. 6. IAR and ACER for the most-effective strategies in Scenarios A–D.

Table 12
Incremental cost-effectiveness ratio for the most-effective strategies.

Strategy	IA $\times 10^6$	Cost	IAR	ACER	ICER
Strategy 1: $u_1(t)$,	2.0679	281.1135	1.5793	1.3594×10^{-4}	1.3594×10^{-4}
Strategy 6: $u_1(t), u_3(t)$	2.1128	1.3487×10^3	1.5239	6.3834×10^{-4}	0.0238
Strategy 14: $u_1(t), u_2(t), u_3(t), u_4(t)$	2.2265	2.0437×10^3	1.4662	9.1789×10^{-4}	0.0061
Strategy 12: $u_1(t), u_2(t), u_4(t)$	2.2265	1.8726×10^3	1.4706	8.4107×10^{-4}	–

Table 13
Incremental cost-effectiveness ratio for the most-effective strategies.

Strategy	IA $\times 10^6$	Cost	IAR	ACER	ICER
Strategy 1: $u_1(t)$,	2.0679	281.1135	1.5793	1.3594×10^{-4}	1.3594×10^{-4}
Strategy 14: $u_1(t), u_2(t), u_3(t), u_4(t)$	2.2265	2.0437×10^3	1.4662	9.1789×10^{-4}	0.0111
Strategy 12: $u_1(t), u_2(t), u_4(t)$	2.2265	1.8726×10^3	1.4706	8.4107×10^{-4}	–

ACER value, followed by Strategy 14, then Strategy 11, which has the highest ACER value. Therefore, Strategy 1 is also the most cost-effective strategy among all the 14 control strategies considered in this paper.

It remains to compare Strategies 1, 6, 12 and 14 using the ICER cost analysis technique. To do this, the control strategies are ranked in increasing order of their effectiveness according to the total number of infections averted (IA) as given in Table 12.

The calculation of ICER is as follows:

$$\text{ICER}(1) = \frac{281.1135}{2.0679 \times 10^6} = 1.3594 \times 10^{-4},$$

$$\text{ICER}(6) = \frac{1.3487 \times 10^3 - 281.1135}{2.1128 \times 10^6 - 2.0679 \times 10^6} = 0.0238,$$

$$\text{ICER}(14) = \frac{2.0437 \times 10^3 - 1.3487 \times 10^3}{2.2265 \times 10^6 - 2.1128 \times 10^6} = 0.0061.$$

Note also that, due the equal number of infection averted by Strategies 14 and 11, the ICER is not compared between these strategies. The summary of the results is given in Table 12. Table 12 reveals a cost-saving of \$0.0061 for Strategy 14 over Strategy 6 based on the comparison of ICER(14) and ICER(6). The lower ICER value obtained for Strategy 14 indicates that Strategy 6 is strongly dominated, more costly and less effective to implement than Strategy 14. Thus, Strategy 6 is discarded from the set of alternative control interventions. The ICER is then calculated for Strategy 1 and Strategy 14 as iterated below and shown in Table 13.

$$\text{ICER}(1) = \frac{281.1135}{2.0679 \times 10^6} = 1.3594 \times 10^{-4},$$

$$\text{ICER}(14) = \frac{2.0437 \times 10^3 - 281.1135}{2.2265 \times 10^6 - 2.0679 \times 10^6} = 0.0111.$$

Table 13 reveals a cost-saving of $\$1.3594 \times 10^{-4}$ for Strategy 1 over Strategy 14 based on the comparison of ICER(1) and ICER(14). The lower ICER value obtained for Strategy 1 indicates that Strategy 14 is strongly dominated, more costly and less effective to implement than Strategy 1. Thus, Strategy 14 is discarded from the set of alternative control interventions. The ICER is then recalculated for Strategy 1 and Strategy 12 as iterated below and shown in Table 14.

$$\text{ICER}(1) = \frac{281.1135}{2.0679 \times 10^6} = 1.3594 \times 10^{-4},$$

$$\text{ICER}(12) = \frac{1.8726 \times 10^3 - 281.1135}{2.2265 \times 10^6 - 2.0679 \times 10^6} = 0.0100.$$

Table 14 reveals a cost-saving of $\$1.3594 \times 10^{-4}$ for Strategy 1 over Strategy 12 following the comparison of ICER(1) and ICER(12). The lower ICER value obtained for Strategy 1 indicates that Strategy 12 is strongly dominated, more costly and less effective to implement than Strategy 1. Therefore, comparing the strategies in scenarios A-D, we conclude that, Strategy 1 will be the most cost-saving and most effective control intervention in the Kingdom of Saudi Arabia. However, in terms of the infection averted, strategy 6, strategy 11, and strategy 12 and strategy 14 are just as good as strategy 1.

Hence, from these analyses, we see that when one considers the following controls: u_1-practising physical or social distancing protocols; u_2-practising personal hygiene by cleaning contaminated surfaces with alcohol-based detergents; u_3-practising proper and safety measures by exposed, asymptomatic infected and asymptomatic infected individuals; u_4-fumigating schools in all levels of education, sports facilities and commercial areas such as markets and public toilet facilities in Kingdom of Saudi Arabia. u_1 (practising physical or social distancing protocols) has the lowest incremental cost-effectiveness and, therefore, gives the optimal cost on a large scale than all the other strategies.

Table 14
Incremental cost-effectiveness ratio for the most-effective strategies.

Strategy	IA $\times 10^6$	Cost	IAR	ACER	ICER
Strategy 1: $u_1(t)$,	2.0679	281.1135	1.5793	1.3594×10^{-4}	1.3594×10^{-4}
Strategy 12: $u_1(t), u_2(t), u_4(t)$	2.2265	1.8726×10^3	1.4706	8.4107×10^{-4}	0.0100

Concluding remarks

We formulated an optimal control model for the model proposed in [20]. We used four COVID-19 controls in the absence of vaccination thus, practising physical or social distancing protocols; practising personal hygiene by cleaning contaminated surfaces with alcohol-based detergents; practising proper and safety measures by exposed, asymptomatic infected and asymptomatic infected individuals; and fumigating schools in all levels of education, sports facilities and commercial areas such as markets and public toilet facilities in Kingdom of Saudi Arabia. The implementation of all the control shows that the disease can be reduced when individuals strictly stick to the proposed controls in this work. The efficacy plots in Fig. 5(b) shows that the controls become much more effective after 39 days. We noticed that, in the pool of the four controls, control u_1 (practising physical or social distancing protocols) and control u_2 (practising personal hygiene by cleaning contaminated surfaces with alcohol-based detergents) should be applied at a constant level throughout, with much effort placed on control u_1 for 98 days. For the control u_3, we noticed that the control should be kept at 0.75 for 25 days and then gradually reduced to 0.29 for the rest of the simulation time. The control profile for control u_4 shows that the control term should be kept for 0.75 for 18 days and then gradually reduced to 0.29 for the rest of the simulation period. We also calculated the infection averted ratio (IAR), average cost-effectiveness ratio (ACER) and the incremental cost-effectiveness ratio (ICER). We also utilized the cost-minimization analysis when it becomes evident that strategies 11, 12, and 14 had the same number of infection averted.

CRediT authorship contribution statement

Joshua Kiddy K. Asamoah: Conceptualization, Investigation, Formal analysis, Cost-effectiveness analysis, Numerical simulations, Writing – review & editing. **Eric Okyere:** Conceptualization, Investigation, Formal analysis, Cost-effectiveness analysis, Writing – review & editing. **Afeez Abidemi:** Conceptualization, Investigation, Formal analysis, The existence of the optimal control model, Cost-effectiveness, Writing – review & editing. **Stephen E. Moore:** Conceptualization, Writing – review & editing. **Gui-Quan Sun:** Conceptualization, Investigation, Formal analysis, Cost-effectiveness analysis, Supervision, Funding acquisition, Writing – review & editing. **Zhen Jin:** Supervision, Writing – review & editing. **Edward Acheampong:** Writing – review & editing. **Joseph Frank Gordon:** Writing – review & editing.

Declaration of competing interest

The authors declare that they have no known competing financial interests or personal relationships that could have appeared to influence the work reported in this paper.

Funding

This work was funded by the National Natural Science Foundation of China under the Grant number: 12022113, Henry Fok Foundation for Young Teachers (171002).

References

[1] Piovella N. Analytical solution of SEIR model describing the free spread of the COVID-19 pandemic. Chaos Solitons Fractals 2020;140:110243.
[2] Arino J, Portet S. A simple model for COVID-19. Infect Dis Model 2020;5:309.
[3] Wangping J, Ke H, Yang S, Wenzhe C, Shengshu W, Shanshan Y, et al. Extended SIR prediction of the epidemics trend of COVID-19 in Italy and compared with Hunan, China. Front Med 2020;7:169.
[4] Cui Q, Hu Z, Li Y, Han J, Teng Z, Qian J. Dynamic variations of the COVID-19 disease at different quarantine strategies in wuhan and mainland China. J Infect Public Health 2020;13:849–55.
[5] Hu L, Nie L-F. Dynamic modeling and analysis of COVID-19 in different transmission process and control strategies. Math Methods Appl Sci 2020;1–14.
[6] Mushayabasa S, Ngarakana-Gwasira ET, Mushanyu J. On the role of governmental action and individual reaction on COVID-19 dynamics in South Africa: A mathematical modelling study. Inform Med Unlocked 2020;20:100387.
[7] Garba SM, Lubuma JM-S, Tsanou B. Modeling the transmission dynamics of the COVID-19 pandemic in south africa. Math Biosci 2020;328:108441.
[8] Atangana A. Mathematical model of survival of fractional calculus, critics and their impact: How singular is our world?. 2021.
[9] Fatima B, Zaman G, Alqudah MA, Abdeljawad T. Modeling the pandemic trend of 2019 Coronavirus with optimal control analysis. Results Phys 2020;103660.
[10] Ali M, Shah STH, Imran M, Khan A. The role of asymptomatic class, quarantine and isolation in the transmission of COVID-19. J Biol Dyn 2020;14(1):389–408.
[11] Atangana A, Araz SI. Modeling and forecasting the spread of COVID-19 with stochastic and deterministic approaches: Africa and Europe. Adv Difference Equ 2021;2021(1):1–107.
[12] Asamoah JKK, Bornaa C, Seidu B, Jin Z. Mathematical analysis of the effects of controls on transmission dynamics of SARS-CoV-2. Alex Eng J 2020;59(6):5069–78. http://dx.doi.org/10.1016/j.aej.2020.09.033.
[13] Atangana A. Modelling the spread of COVID-19 with new fractal-fractional operators: can the lockdown save mankind before vaccination? Chaos Solitons Fractals 2020;136:109860.
[14] Lemecha Obsu L, Feyissa Balcha S. Optimal control strategies for the transmission risk of COVID-19. J Biol Dyn 2020;14(1):590–607.
[15] Aldila D, Ndii MZ, Samiadji BM. Optimal control on COVID-19 eradication program in Indonesia under the effect of community awareness. Aims Press; 2020.
[16] Deressa CT, Duressa GF. Modeling and optimal control analysis of transmission dynamics of COVID-19: The case of Ethiopia. Alex Eng J 2020.
[17] Perkins A, Espana G. Optimal control of the COVID-19 pandemic with non-pharmaceutical interventions. Bull Math Biol 2020;82:118.
[18] Oud MAA, Ali A, Alrabaiah H, Ullah S, Khan MA, Islam S. A fractional order mathematical model for COVID-19 dynamics with quarantine, isolation, and environmental viral load. Adv Difference Equ 2021;2021(1):1–19.
[19] Asamoah JKK, Owusu MA, Jin Z, Oduro F, Abidemi A, Gyasi EO. Global stability and cost-effectiveness analysis of COVID-19 considering the impact of the environment: using data from Ghana. Chaos Solitons Fractals 2020;140:110103. http://dx.doi.org/10.1016/j.chaos.2020.110103.
[20] Alqarni MS, Alghamdi M, Muhammad T, Alshomrani AS, Khan MA. Mathematical modeling for novel coronavirus (COVID-19) and control. Nume Methods Partial Differential Equ 2020.
[21] Seidu B. Optimal strategies for control of COVID-19: A mathematical perspective. Scientifica 2020;2020.
[22] Asamoah JKK, Jin Z, Sun G-Q, Seidu B, Yankson E, Abidemi A, et al. Sensitivity assessment and optimal economic evaluation of a new COVID-19 compartmental epidemic model with control interventions. Chaos Solitons Fractals 2021;146:110885. http://dx.doi.org/10.1016/j.chaos.2021.110885.
[23] Omame A, Sene N, Nometa I, Nwakanma CI, Nwafor EU, Iheonu NO, et al. Analysis of COVID-19 and comorbidity co-infection model with optimal control. MedRxiv 2020.
[24] Van den Driessche P, Watmough J. Reproduction numbers and sub-threshold endemic equilibria for compartmental models of disease transmission. Math Biosci 2002;180(1–2):29–48.
[25] Asamoah JKK, Oduro FT, Bonyah E, Seidu B. Modelling of rabies transmission dynamics using optimal control analysis. J Appl Math 2017;2017. http://dx.doi.org/10.1155/2017/2451237.
[26] Agusto F, Leite M. Optimal control and cost-effective analysis of the 2017 meningitis outbreak in nigeria. Infect Dis Model 2019;4:161–87.
[27] Berhe HW. Optimal control strategies and cost-effectiveness analysis applied to real data of cholera outbreak in Ethiopia's Oromia region. Chaos Solitons Fractals 2020;138:109933.
[28] Abidemi A, Aziz NAB. Optimal control strategies for dengue fever spread in johor, Malaysia. Comput Methods Prog Biomed 2020;105585.
[29] Abidemi A, Ahmad R, Aziz NAB. Global stability and optimal control of dengue with two coexisting virus serotypes. MATEMATIKA: Malays J Ind Appl Math 2019;35(4):149–70.

[30] Asamoah JKK, Jin Z, Sun G-Q. Non-seasonal and seasonal relapse model for Q fever disease with comprehensive cost-effectiveness analysis. Results Phys 2021;103889. http://dx.doi.org/10.1016/j.rinp.2021.103889.
[31] Olaniyi S, Obabiyi O, Okosun K, Oladipo A, Adewale S. Mathematical modelling and optimal cost-effective control of COVID-19 transmission dynamics. Eur Phys J Plus 2020;135(11):1–20.
[32] Asamoah JKK, Jin Z, Sun G-Q, Li MY. A deterministic model for Q fever transmission dynamics within dairy cattle herds: Using sensitivity analysis and optimal controls. Comput Math Methods Med 2020;2020. http://dx.doi.org/10.1155/2020/6820608.
[33] Asamoah JKK, Nyabadza F, Jin Z, Bonyah E, Khan MA, Li MY, et al. Backward bifurcation and sensitivity analysis for bacterial meningitis transmission dynamics with a nonlinear recovery rate. Chaos Solitons Fractals 2020;140:110237. http://dx.doi.org/10.1016/j.chaos.2020.110237.
[34] Asamoah JKK, Nyabadza F, Seidu B, Chand M, Dutta H. Mathematical modelling of bacterial meningitis transmission dynamics with control measures. Comput Math Methods Med 2018;2018. http://dx.doi.org/10.1155/2018/2657461.
[35] Okyere E, Olaniyi S, Bonyah E. Analysis of Zika virus dynamics with sexual transmission route using multiple optimal controls. Sci Afr 2020;9:e00532.
[36] Berhe HW, Makinde OD, Theuri DM. Optimal control and cost-effectiveness analysis for dysentery epidemic model. Appl Math Inform Sci 2018;12:1183–95.
[37] Olaniyi S, Okosun K, Adesanya S, Lebelo R. Modelling malaria dynamics with partial immunity and protected travellers: optimal control and cost-effectiveness analysis. J Biol Dyn 2020;14(1):90–115.
[38] Rector CR, S C, J D. Principles of optimization theory. New Delhi: Narosa Publishing House; 2005.
[39] Romero-Leiton JP, Montoya Aguilar JM, Ibargüen-Mondragón E. An optimal control problem applied to malaria disease in Colombia. Appl Math Sci 2018;12(6):279–92.
[40] Pontryagin L, Boltyanskii V, Gamkrelidze R, Mishchenko E. The mathematical theory of optimal processes. Wiley, NY; 1962.
[41] Agusto FB, ELmojtaba IM. Optimal control and cost-effective analysis of malaria/visceral leishmaniasis co-infection. PLoS One 2017;12(2):e0171102.
[42] Agusto F. Optimal isolation control strategies and cost-effectiveness analysis of a two-strain avian influenza model. Biosystems 2013;113(3):155–64.